A&A 450, 993–1004 (2006)
DOI: 10.1051/0004-6361:20054003

Astronomy & Astrophysics

Deep X-ray survey of the young open cluster NGC 2516 with XMM-Newton⋆,⋆⋆

I. Pillitteri[1], G. Micela[2], F. Damiani[2], and S. Sciortino[2]

[1] Università degli Studi di Palermo, Piazza del Parlamento 1, 90134 Palermo, Italy
e-mail: pilli@astropa.unipa.it
[2] INAF – Osservatorio Astronomico di Palermo Piazza del Parlamento 1, 90134 Palermo, Italy
e-mail: [giusi;damiani;sciorti]@astropa.unipa.it

Received 6 August 2005 / Accepted 6 January 2006

ABSTRACT

Aims. We report a deep X-ray survey of the young (∼140 Myr), rich open cluster NGC 2516 obtained with the EPIC camera on board the XMM-Newton satellite.
Methods. By combining data from six observations, a high sensitivity, greater than a factor of 5 with respect to recent Chandra observations, has been achieved. Kaplan-Meier estimators of the cumulative X-ray luminosity distribution are built, statistically corrected for non members contaminants and compared to those of the nearly coeval Pleiades. The EPIC spectra of the X-ray brightest stars are fitted using optically thin model plasma with one or two thermal components.
Results. We detected 431 X-ray sources and 234 of them have as optical counterparts cluster stars spanning the entire NGC 2516 Main Sequence. On the basis of X-ray emission and optical photometry, we indicate 20 new candidate members of the cluster; at the same time we find 49 X-ray sources without known optical or infrared counterpart. The X-ray luminosities of cluster stars span the range $\log L_X$ (erg s^{-1}) = 28.4–30.8. The representative temperatures span the 0.3–0.6 keV (3.5–8 MK) range for the cool component and 1.0–2.0 keV (12–23 MK) for the hot one; similar values are found in other young open clusters like the Pleiades, IC 2391, and Blanco 1. While no significant differences are found in X-ray spectra, NGC 2516 solar type stars are definitely less luminous in X-rays than the nearly coeval Pleiades. The comparison with a previous ROSAT survey reveals the lack of variability amplitudes larger than a factor of 2 in solar type stars in a ∼11 yr time scale of the cluster and thus activity cycles like in the Sun are probably absent or have a different period and amplitude in young stars.

Key words. X-ray: stars – stars: activity – open clusters and associations: individual: NGC 2516

1. Introduction

X-ray observations of stars have shown that X-ray emission is a common feature along the main sequence (Vaiana et al. 1981). The emission mechanisms depend on mass: in massive O and early B type stars the X-rays are likely generated by plasma shocked and heated in stellar winds, although a role of the magnetic field is not ruled out (Lucy & White 1980; Feldmeier 1995; Babel & Montmerle 1997; Cassinelli & MacGregor 2000; Waldron & Cassinelli 2001); solar mass stars present coronae composed of hot, magnetically confined emitting plasma, as directly observed in the Sun (Vaiana et al. 1981). Only B-late – A-early stars are not expected to emit significant X-rays because neither strong stellar winds nor convective regions, necessary to have a solar magnetic dynamo, are present in these stars. Focusing on solar mass stars, the X-ray activity is strictly linked to the internal structure and the rotation. The coupling of convective motion and rotation produces the solar-type dynamo. The loss of angular momentum is the main factor leading to a decrease of X-ray activity during stellar evolution, especially in the first Gyr, although the role of other factors like stellar chemical composition or environmental forming conditions cannot be ruled out.

In this context the studies based on stellar open clusters with different properties are of great importance to better define the relevance of age differences, chemical composition and environmental influence. An open cluster like the Pleiades constitutes a prototype for the study of activity and evolution at an age around 100 Myr, given its richness and nearby location. The evolution of X-ray emission with stellar age has been

⋆ Based on observations obtained with XMM-Newton, an ESA science mission with instruments and contributions directly funded by ESA Member States and NASA.
⋆⋆ Appendices A–D are only available in electronic form at http://www.edpsciences.org

Table 1. Log of XMM-Newton observations of NGC 2516. All exposures have been taken with the *Thick* filter. Positions refer to J2000, times (referred to the pn exposures) are in kiloseconds.

OBS Id.	Orbit Nr.	RA	Dec	Time (filtered/total)	Date
0113891001	0060	7:58:20	–60:52:13	20.0/20.0	2000-04-06 @ 19:25:05
0113891101	0060	7:58:20	–60:52:13	14.5/17.0	2000-04-07 @ 04:05:31
0126511201	0092	7:58:22	–60:45:36	21.9/27.5	2000-06-10 @ 08:56:51
0134531201	0209	7:58:22	–60:45:36	18.8/19.0	2001-01-29 @ 00:23:20
0134531301	0209	7:58:22	–60:45:36	9.3/9.3	2001-01-29 @ 08:01:48
0134531501	0346	7:58:22	–60:45:36	21.2/21.2	2001-10-29 @ 09:53:59

studied in the last five years with XMM-Newton and Chandra X-ray observatories, which provided high quality surveys of open clusters like Pleiades, Blanco 1, IC 2391, NGC 6383, NGC 188, M 67 (cf. Briggs & Pye 2003; Pillitteri et al. 2004; Marino et al. 2004; Rauw et al. 2003; van den Berg et al. 2004; Gondoin 2005). In this paper we study the X-ray emission of the young open cluster NGC 2516.

NGC 2516 is a rich open cluster with an age of 140 Myr (Meynet et al. 1993), slightly older than the Pleiades, located in the southern hemisphere at a height of ∼100 pc on the Galactic Plane. The richness of star and its relatively nearby location (about 387 pc) have motivated the growing interest in the study of this cluster both in the optical and in the X-ray band. In the optical band the photometric study of Dachs (1970) and Dachs & Kabus (1989) have shown a higher number of stars and a larger fraction of peculiar Ap stars than the Pleiades. Episodes of subsequent star formation, due to passages across the Galactic Plane or interaction with the Gum Nebula, have been also speculated by Dachs & Kabus (1989) in order to explain younger blue stragglers in this cluster. More recently, the deep photometric survey of Jeffries et al. (2001) allowed one to trace the cluster sequence down to $V \simeq 20$ and to build an optical catalog of 1254 photometric members. The Mass Function of the cluster is consistent with the empirical Salpeter's power law $\mathrm{d}N/\mathrm{d}M \propto M^{-1.35}$ but with index 1.47–1.67, depending on the assumed metallicity. The chemical composition remains uncertain for this cluster: while photometry suggests a significant underabundance of metals ([Fe/H] = –0.3, Jeffries et al. 2001), more recently Terndrup et al. (2002), on the basis of high resolution spectroscopy of two stars, strongly suggested a more solar-like metallicity for NGC 2516. Furthermore, these authors conclude that an age of 150 Myr and a distance modulus of 7.93 mag (i.e. a distance of ∼385.5 pc) are more appropriate.

In the X-ray band Jeffries et al. (1997) and Micela et al. (2000) analyzed ROSAT PSPC and HRI observations leading to 47 detections among cluster stars with spectral type from B2 down to K. The G- and K-type stars of the cluster appeared under-luminous when compared to the Pleiades suggesting the low metallicity of the cluster (estimated at that time by photometry) to have a role in determining the X-ray emission. With the advent of *Chandra* and *XMM-Newton* missions, the cluster has been studied by Harnden et al. (2001), Sciortino et al. (2001) and Damiani et al. (2003), confirming the under-luminosity of solar type stars with respect to the Pleiades and reporting X-ray emission from several Ap stars. In M-type stars the X-ray emission was found similar to the Pleiades. The time X-ray variability of stars in NGC 2516 has been studied by Wolk et al. (2004) with Chandra observations over a 2 year time span.

Unfortunately, cluster membership is determined only through photometry, since cluster proper motion is close to the solar value, making it very difficult to obtain reliable astrometric membership determination. Therefore the low X-ray emission level in solar type stars could be attributed to both a significant contamination of the cluster sample or to a real effect, related to the slightly older age of NGC 2516 with respect to the Pleiades.

In the present paper we report a deep X-ray survey of NGC 2516 obtained through a series of observations with the XMM-Newton satellite. Our aim is to determine with the highest sensitivity the X-ray emission of the cluster. In particular we focus on the X-ray properties of solar type stars of this cluster and their comparison with those of the very similar and well studied Pleiades. The structure of the paper is as follows: in Sect. 2 we present the data and the analysis method. In Sect. 3 we discuss the spectral properties and the X-ray emission level of solar type stars. In Sect. 4 we compare the X-ray luminosities from XMM-Newton with those of Chandra and ROSAT. Sect. 5 gives a discussion on other stars suggested as possible new members of the cluster, based on X-ray emission and optical photometry. In Sect. 6 we give a brief summary of relevant results.

2. The observations and the data analysis

NGC 2516 has been observed several times with XMM-Newton during the first two years of satellite operations for calibration purposes. Table 1 summarizes the relevant information of the observations we have used. They span a period of 19 months with exposure times between 10 and 20 ks. All of these observations have been performed with the thick filter. Figure 1 shows the summed EPIC exposures (left panel) and the optical image of the same region (right panel).

The data of each EPIC detector (MOS 1, 2 and pn) have been reduced with SAS software in order to obtain tables of photons with calibrated astrometry, arrival times and energies. Subsequently we have chosen only events in the EPIC field of view, with energies in the 0.3–7.9 keV band, and that have triggered up to four pixels simultaneously. The data have been screened from high background rate intervals by maximizing the signal-to-noise ratio of weak sources. Figure 2 shows an example of the time screening procedure for EPIC pn of

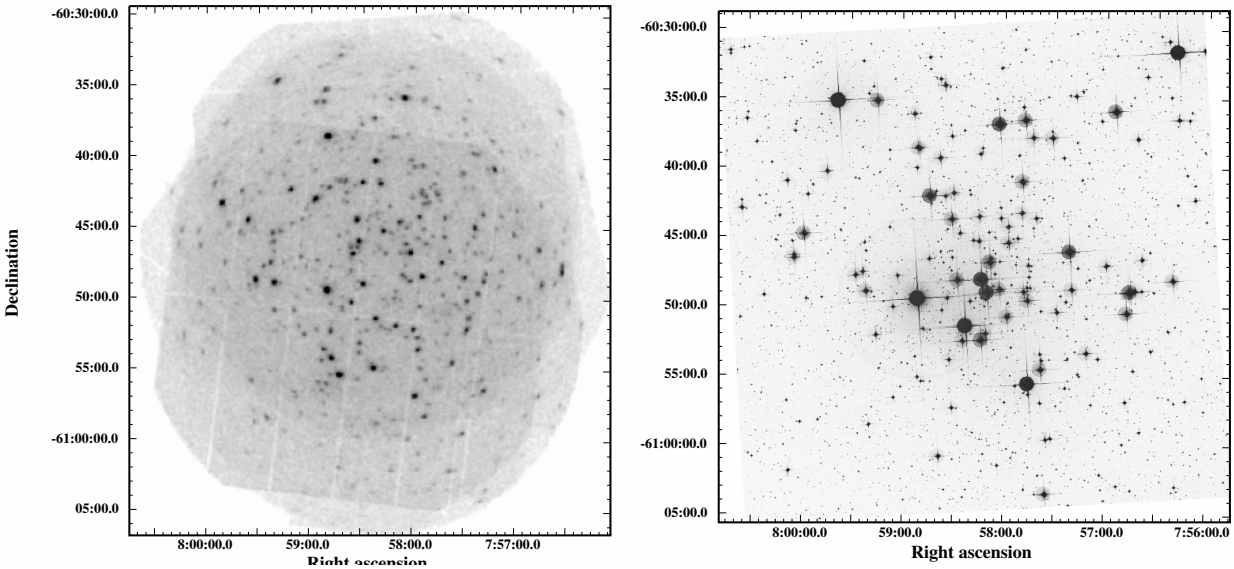

Fig. 1. X-ray (*left panel*) and optical (*right panel*) images of the NGC 2516 cluster. The X-ray survey covers a sky region of $\sim 18' \times 25'$ and contains 593 cluster stars (cf. Sect. 2.1).

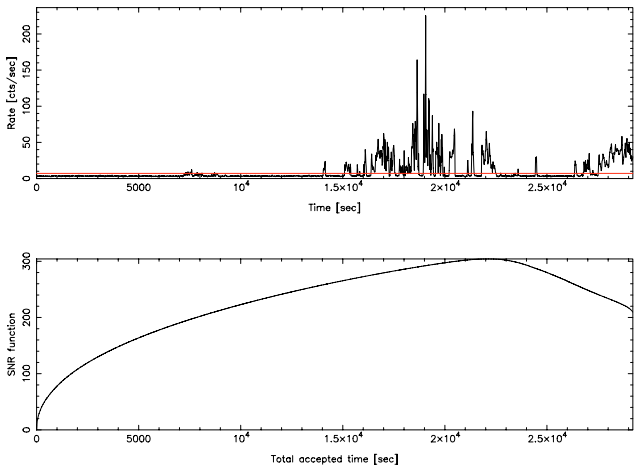

Fig. 2. Light curve for MOS 1 of EPIC observation during the XMM orbit 0092 (*top panel*); the horizontal line is the threshold rate that corresponds to filter the event times in order to maximize the S/N function, plotted in the bottom panel as a function of the total accepted times.

observation during the orbit 0092, the worst case in our set of observations. The light curve of all photons is plotted in the top panel. Spikes are due to intervals of high background. The bottom panel shows the signal to noise ratio as a function of time. We have chosen a rate threshold that filters only the time intervals yielding the maximum signal to noise ratio in the filtered image in order to optimize the detection of the weakest sources. The derived fraction of exposure for each observation (pn exposures only) is reported in Table 1.

Source detection and X-ray photometry derived from the sum of all the MOS and pn exposures have been obtained with PWXDetect code, developed at the INAF – Osservatorio Astronomico di Palermo, derived from the original ROSAT code for source detection (Damiani et al. 1997a,b) and based on the analysis of the wavelet transform of the count rate image. It allows one to combine data from different EPIC detectors taken in different observations in order to achieve the deepest sensitivity. The code provides estimates of the positions, total counts, rates, effective exposure times and significance of each detection.

We have chosen MOS 1 as a reference detector to evaluate rates, fluxes and luminosities. The scaling factor between MOS 1, MOS 2 and pn depends on the source spectrum, the filter used during observation and the chosen energy band. In order to properly scale the rates of pn to MOS1 despite the different efficiency, we have used the ratios of source count rates, as deduced by photons accumulated in a 15″ radius circular region at the source positions. In this way we directly use the data to find the relative instrument efficiencies without any hypotheses about the source spectrum. The rates in the summed image are equivalent to MOS 1 count rates (CR) according to the following formula:

$$\begin{aligned} \mathrm{CR_{sum}} &= \Sigma_{\mathrm{MOS1}}\mathrm{CR_{MOS1}} \\ &\quad + \Sigma_{\mathrm{MOS2}}\mathrm{CR_{MOS2}} \cdot r_{\mathrm{MOS2/MOS1}} + \Sigma\mathrm{CR_{pn}} \cdot r_{\mathrm{pn/MOS1}} \end{aligned}$$

where the medians of the scaling factors $r_{\mathrm{MOS2/MOS1}}$ and pn/MOS1 are respectively ∼1 and ∼3.6, as evaluated from source count rates measured by different detectors. The exposure times used to calculate CRs are obtained from exposure maps, and thus they take into account any spatial non-uniformities due to vignetting, RGS grating obscuration, chip geometry etc.

In the combined EPIC datasets we have detected 431 X-ray sources with a significance level greater than 5.0σ, which should lead statistically to at most one spurious source in the field of view. The threshold has been calibrated by applying the source detection algorithm to 500 simulated datasets of only background photons. In Table A.1 we report the list of sources and their properties.

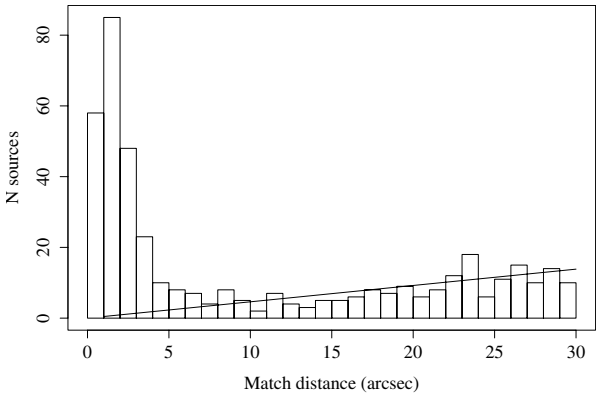

Fig. 3. Histogram of offsets between X-ray sources and the optical members positions of NGC 2516. The line traces the distribution of expected spurious matches.

2.1. X-rays from NGC 2516: fluxes and luminosities

The optical catalog of NGC 2516 was built from the list of 1254 photometric members compiled by Jeffries et al. (2001). The member selection is based on the photometry in the B, V and I bands, and 551 stars of this catalog lie in the combined field of view of the 6 XMM observations. We have added to this catalog 42 cluster stars from Dachs & Kabus (1989) brighter than $V = 9.7$, not present in the Jeffries et al. (2001) sample. This sample covers a $\sim 58' \times 54'$ sky region, whereas the combined EPIC image covers only about $18' \times 25'$, centered on the core of the cluster (cf. Fig. 1). The number of cluster stars in the surveyed area is 593. We will refer to the stars of this catalog as JTH with a running number, while for the optically bright stars we will also use the DK acronym from Dachs & Kabus (1989).

We have matched the positions of X-ray sources with the optical coordinates of the composite catalog. No significant systematic offsets were found between optical and X-ray astrometry. By studying the distribution of the distances of matched sources, we have chosen a maximun identification radius of $7''$ where the number of observed matches is similar to the number of expected chance identifications. We can estimate the expected number of chance matches uncorrelated with true cluster members at a given threshold distance by taking into account the star density of the optical catalog in the EPIC field of view and the number of X-ray detections to be matched; it yields 12 false matches at the chosen $7''$ radius, by integrating the line traced in Fig. 3. The value of the adopted radius does not change significantly when matching the X-ray sources at small and large off axis positions. A list of 239 matches with the optical catalog was obtained; five X-ray sources were doubly matched with close pairs in the optical catalog; 354 cluster members in the surveyed area remain undetected in X-rays and thus we have calculated upper limits to their X-ray count rates, fluxes and luminosities at the chosen detection threshold at the positions of undetected stars. Tables B.1 and C.1 list the detected stars and the upper limits for the cluster stars, respectively.

We have estimated a conversion factor (CF) in the 0.3–7.9 keV band between count rates (in units of the MOS 1 instrument, as obtained by the detection code) and unabsorbed fluxes, derived by the spectral analysis of the bright X-ray sources of the cluster (see Sect. 2.3); the resulting CF, used for all the cluster X-ray sources, was 9.5×10^{-12} erg cnt^{-1} cm^{-2}. The 3 sigma uncertainty on the CF takes into account the dependence on the spectrum hardness and is ±14%; it would systematically shift fluxes and luminosities by +0.06 and –0.07 dex, respectively.

To obtain the luminosities we assumed a distance to the cluster of 387 pc, as adopted by Jeffries et al. (1997) and Damiani et al. (2003). This distance is slightly larger than the *Hipparcos* satellite estimate (346 pc); by assuming this latter the luminosities would decrease by –0.05 dex. Table 2 reports the number and the rate of detections for each spectral type (indeed for each range of $B - V$ or $V - I$ color as reported in the header of the table), the number of stars in the field of view, the medians of X-ray luminosities, also after correction for non members contamination (see Sect. 3.3) and the minimum of detected luminosity. The weakest source of the cluster is a M-type star, with a X-ray flux equal to 1.2×10^{-15} erg s^{-1} cm^{-2} and luminosity of 2.2×10^{28} erg s^{-1}. For comparison the Chandra survey of Damiani et al. (2003) led to a minimum detected flux among cluster sources of 2.75×10^{-15} erg s^{-1} cm^{-2} in a very similar band. The choice of the CF and the distance does not result in a systematic difference between the luminosities obtained in the present survey and that of Damiani et al. (2003) conducted with Chandra (cf. Fig. 9); in Sect. 4 we discuss in detail the comparison of luminosities estimated with Chandra and XMM-Newton.

2.2. Uncertainties on X-ray fluxes and luminosities

We summarize here all the statistical and systematic errors that could affect our estimates of fluxes and luminosities. Count rates have relative errors in the 5%–30% range (as reported in Table A.1). The CF has a 14% uncertainty at 3σ level from fit of fluxes vs. count rates, essentially due to the effect of source spectrum temperature on CF. The scaling of pn to MOS introduces an uncertainty of ∼11% i.e. fluxes and luminosities can be systematically higher or lower by –0.03 or +0.015 dex, respectively. The different distance estimates given in the literature should systematically shift the X-ray luminosities by –0.05 (346 pc, Hipparcos distance) or +0.022 (for a distance of 407 pc, Terndrup et al. 2002). All these sources of uncertainties could balance themselves, the errors in Table B.1 may suffer an additional systematic uncertainty of ∼±0.07 dex in flux and ±0.08 dex in luminosities.

2.3. Spectral analysis

We used EPIC data to investigate the spectral properties of the NGC 2516 stellar coronae in terms of relevant temperatures and emission measures. The pn has the highest efficiency in collecting X-ray photons among the three EPIC instruments, hence we have used the data from each pn exposure by simultaneously fitting the X-ray spectra observed in different

Table 2. Number of X-ray detections, number of stars in the EPIC field of view, medians of $\log L_X$ distributions (we report also the values corrected for non member contaminants in G-, K- and M-type stars, see Sect. 3.3) and minimum detected luminosity for B, A-, F-, G-, K- and M-type stars of NGC 2516. The selection of the spectral types is reported in the table header. In cases where the rate of detection is <50% only an upper limit to the median is reported.

Sp. Type	B	A	F	G	K	M
	$(B-V)_0 < 0$	$0 \le (B-V)_0 \le 0.3$	$0.3 \le (B-V)_0 \le 0.5$	$0.5 \le (B-V)_0 \le 0.8^a$	$0.93 \le (V-I)_0 \le 2.2$	$2.2 \le (V-I)_0 \le 5.0$
N_{det}/N_{tot}	13/38	16/49	24/37	52/89	74/182	59/194
Detect. Rate	34%	33%	65%	58%	41%	30%
$\log L_X$ median	≤28.62	≤28.44	29.19	28.95	≤28.70	≤28.62
$\log L_X$ med.$_{nocont.}$	...	...	...	29.04	≤28.82	≤28.68
Min Det $\log L_X$	28.85	28.60	28.71	28.55	28.5	28.34

[a] Combined with: $(V-I)_0 \le 0.93$.

Table 3. Temperatures and emission measures estimated from global fits of coronal spectra. Models with 1-T or 2-T components have been used, errors refer to 10%–90% χ^2 confidence range.

Num	$B-V$	T_1 (keV)	T_2 (keV)	log EM$_1$ (cm^{-3})	log EM$_2$ (cm^{-3})	χ^2/d.o.f.
9465	0.818	$0.72^{0.07}_{-0.08}$	$1.69^{0.5}_{-0.3}$	$52.93^{0.04}_{-0.17}$	$53.06^{0.02}_{-0.17}$	2.7/88
9676	0.903	$0.34^{0.09}_{-0.07}$	$1.14^{0.13}_{-0.11}$	$52.79^{0.02}_{-0.2}$	$52.94^{0}_{-0.13}$	2.4/95
7678	0.928	$0.37^{0.13}_{-0.08}$	$1.59^{0.7}_{-0.3}$	$52.6^{0.04}_{-0.24}$	$52.63^{0.03}_{-0.18}$	2.3/25
7782	1.417	$0.28^{0.1}_{-0.09}$	$1.25^{0.5}_{-0.3}$	$52.69^{0.05}_{-0.5}$	$52.99^{0.04}_{-0.13}$	4.5/7
9175	0.585	$0.66^{0.09}_{-0.07}$	–	$53.2^{0.1}_{-0.2}$	–	3.5/15
8893	1.433	$0.32^{0.3}_{-0.06}$	$1.29^{0.15}_{-0.15}$	$52.51^{0.08}_{-0.2}$	$52.73^{0.03}_{-0.1}$	2.3/42
11 233	0.834	$0.6^{0.08}_{-0.2}$	$1.2^{0.2}_{-0.2}$	$52.91^{0.09}_{-0.14}$	$52.86^{0.06}_{-0.16}$	1.3/55
6649	0.817	$0.56^{0.24}_{-0.25}$	$1.3^{0.3}_{-0.2}$	$52.22^{0.4}_{-0.2}$	$52.78^{0.08}_{-0.2}$	1.1/23
7585	0.719	$0.6^{0.07}_{-0.2}$	$2.04^{1.1}_{-0.6}$	$52.68^{0.07}_{-0.3}$	$52.68^{0.04}_{-0.13}$	1.4/26
4598	0.861	$0.7^{0.1}_{-0.1}$	$2.1^{0.9}_{-0.5}$	$52.96^{0.04}_{-0.2}$	$53.16^{0.1}_{-0.21}$	1.3/28
9140	0.736	$0.74^{0.07}_{-0.14}$	$1.7^{2.5}_{-0.7}$	$52.85^{0.04}_{-0.2}$	$52.54^{0.2}_{-0.6}$	1.35/26
7864	0.603	$0.7^{0.4}_{-0.4}$	$1.6^{8.4}_{-0.5}$	$52.5^{0.2}_{-0.7}$	$52.8^{0.09}_{-0.5}$	0.3/6
8997	0.981	$0.8^{0.2}_{-0.1}$	–	$52.85^{-0.01}_{-0.11}$	–	2.0/38
8458	0.533	$0.54^{0.04}_{-0.06}$	–	$52.92^{-0.01}_{-0.1}$	–	1.2/47
8099	0.56	$0.61^{0.05}_{-0.05}$	–	$52.81^{-0.02}_{-0.11}$	–	2.1/20
9054	0.691	$0.32^{0.06}_{-0.09}$	$0.9^{0.09}_{-0.15}$	$52.73^{0.1}_{-0.1}$	$52.65^{0.09}_{-0.06}$	1.6/49
7667	0.195	$0.60^{0.4}_{-0.04}$	–	$52.66^{0.05}_{-0.05}$	–	1.7/26
10 046	0.99	$0.31^{0.05}_{-0.05}$	$1.5^{0.3}_{-0.3}$	$52.81^{-0.01}_{-0.3}$	$52.93^{0.02}_{-0.1}$	0.7/16
8529	0.583	$0.64^{0.06}_{-0.04}$	–	$52.85^{-0.03}_{-0.1}$	–	2.1/24
8886	0.113	$0.32^{0.17}_{-0.2}$	$3.5^{1.7}_{-1.0}$	$52.3^{1.3}_{-0.7}$	$52.9^{0.1}_{-0.1}$	0.7/22
6029	0.674	$0.4^{0.2}_{-0.1}$	$1.3^{1.1}_{-0.3}$	$52.92^{0.05}_{-0.2}$	$52.7^{0.01}_{-0.3}$	1.8/19
8634	0.943	$0.38^{0.14}_{-0.07}$	$1.21^{0.14}_{-0.15}$	$52.79^{0.01}_{-0.2}$	$52.92^{-0.02}_{-0.16}$	1.0/34
9835	0.988	$0.14^{0.11}_{-0.13}$	$0.94^{0.13}_{-0.12}$	$52.9^{1.2}_{-0.6}$	$52.91^{-0.03}_{-0.2}$	2.4/14
10 817	0.525	$0.59^{0.16}_{-0.17}$	11^{6}_{-6}	$53.02^{0.05}_{-0.3}$	$53.48^{0.05}_{-0.07}$	1.4/16
8641	1.063	$0.37^{0.13}_{-0.07}$	$0.99^{0.09}_{-0.09}$	$52.91^{0.02}_{-0.23}$	$52.99^{0.01}_{-0.12}$	1.4 /64
7743	0.655	$0.73^{0.07}_{-0.09}$	–	$52.82^{-0.01}_{-0.13}$	–	1.0/12
DK23	0.06	$0.56^{0.06}_{-0.12}$	–	$51.6^{1.0}_{-0.2}$	–	1.6/21
DK44B	–0.02	$0.73^{0.07}_{-0.11}$	–	$52.68^{0.05}_{-0.05}$	–	1.5/24
DK56	–0.09	$0.8^{0.2}_{-0.1}$	$3^{0.7}_{-0.4}$	$52.56^{0.09}_{-0.2}$	$53.29^{0.04}_{-0.04}$	0.9/99
DK73	0.02	$0.6^{0.1}_{-0.07}$	–	$52.69^{0.07}_{-0.05}$	–	1.5 /19
DK62	0.03	$0.61^{0.05}_{-0.2}$	$1.4^{0.5}_{-0.3}$	$52.76^{0.08}_{-0.18}$	$52.81^{0.11}_{-0.17}$	1.5/39
6689	0.329	$0.73^{0.12}_{-0.11}$	–	$53.43^{0.11}_{-0.16}$	–	1.4/10
9852	0.659	$0.54^{0.06}_{-0.07}$	–	$53.0^{0.2}_{-0.5}$	–	2.2/19
7650	0.62	$0.6^{0.1}_{-0.1}$	–	$53.0^{0.2}_{-0.3}$	–	1.1/6
8660	0.571	$0.59^{0.08}_{-0.1}$	–	$53.1^{0.3}_{-0.2}$	–	3.8/12
10 040	1.034	$0.76^{0.09}_{-0.1}$	–	$53.22^{0.15}_{-0.15}$	–	0.9/12
9882	0.185	$0.65^{0.06}_{-0.06}$	–	$53.1^{0.2}_{-0.3}$	–	1.1/13
8967	0.996	$0.75^{0.17}_{-0.17}$	–	$53.24^{0.2}_{-0.17}$	–	0.7/5

exposures[1]. In order to perform a spectral analysis with a global fitting technique. we have accumulated the spectra for sources with more than 500 total counts in the sum of datasets. For 31 sources with more than 1000 counts in the summed image, the photons were extracted within a 30″ radius circular region centered at the position of the source, and the background spectrum was accumulated in annuli (with radii of 35″ and 45″, respectively).

For 7 sources with counts between 500 and 1000 total counts we chose to accumulate counts in a 20″ radius region and to fit spectra without background subtraction, considering that background photons are reduced to 44% in this area with respect to the area of radius 30″, whereas the source encircled energy is reduced from 80% to ≃70%. In this way we expect to reduce the contamination of the background spectrum and to save most of the source photons without increasing the uncertainties due to background subtraction. We have tested this procedure in a few cases finding that the background subtraction increases the relative error of fitted parameters by more than 30%, while the best fit temperature slightly decreases within the uncertainty range. The background photons are ∼60 ± 30 in the 20″ extraction area, the actual number depending on the source off-axis distance. We have also included sources with only 500 counts to reduce possible biases introduced by considering only higher count statistics, hence higher activity stars.

The spectra of sources with the highest statistics were fit in most cases with a sum of two APEC models plus photoelectric absorption. After having tried models with the absorption and the abundance as free parameters, we fix the column density value to $N_{\rm H} = 8 \times 10^{20}$ cm^{-2}, consistent with estimates from photometry (Jeffries et al. 2001), and the abundances to those at 0.3 $Z_{\odot}$ because we noticed that under-solar abundances are always obtained, leaving thus as free parameters the two temperatures and emission measures. The spectra of low statistics sources were fit with one APEC model, with as free parameters the temperature, abundance and emission measure and a fixed absorption at $N_{\rm H} = 8 \times 10^{20}$ cm^{-2}, as chosen before. Results from spectral fitting are reported in Table 3 and discussed in Sect. 3.2; errors refer to the 10%–90% χ^2 confidence range.

3. Discussion

3.1. X-ray emission along the main sequence

Figure 4 shows the color–magnitude diagrams (CMD) in B, V, I bands for the photometric cluster members. Hotter stars are shown only in the left panel (CMD with $B - V$) while cooler stars with unreliable $B - V$ are shown only in the CMD with $V-I$ color index. The X-ray detections span the Main Sequence of the cluster from B type stars down to cool, low mass M-type stars.

[1] In some cases we have excluded spectra with very few photons so for each source we do not always fit simultaneously all the spectra from the six observations.

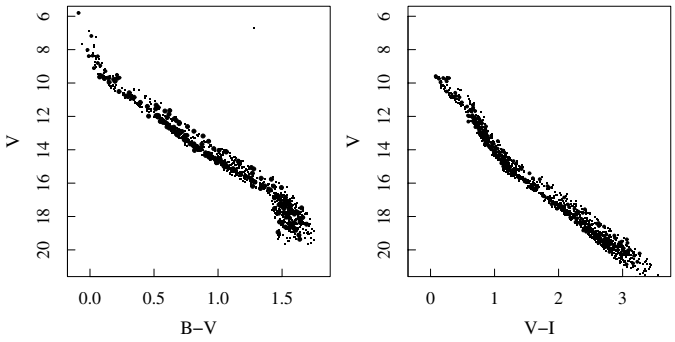

Fig. 4. Color–magnitude diagrams in B, V, I bands of NGC 2516 stars (small dots) from Jeffries et al. (2001) and Dachs & Kabus (1989). Large dots are X-ray detected stars.

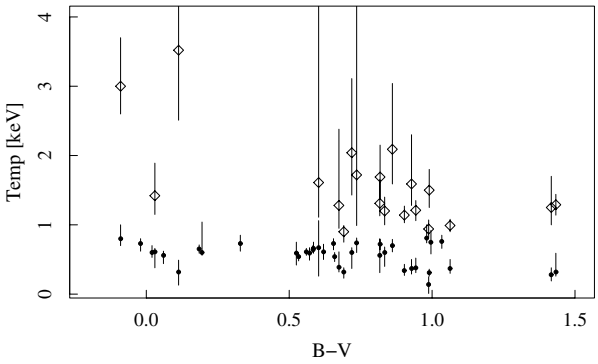

Fig. 5. Coronal temperatures as a function of $B - V$ color. Filled dots refer to the cool component whereas empty diamonds refer to the hot component.

3.2. X-ray spectral properties

The sample of stars for which we have analyzed the spectra contains by solar G- and K- type stars and hot, massive B- and early A- type stars. We were unable to analyze the spectra of stars with $B - V \sim 0.4$ (late-A spectral type stars) because of their lower X-ray fluxes and hence spectra with poor statistical significance. The models we used are too simple and unrealistic; a distribution of plasma temperatures would be more realistic. However we can determine the dominant temperatures of the coronae as is usually done with low resolution X-ray spectra.

In Fig. 5 we plot the temperatures derived from global fitting as a function of $B-V$ color. We were able to fit most of the spectra of solar type stars with 2 temperature models. High energy tails of spectra have very few photons, consequently hot components have been estimated with large errors. The temperatures are in the 0.3–0.7 keV and 1.0–2.0 keV range, and are similar to those detected in the coronae of Pleiades and Blanco 1 open clusters, which are nearly coeval to NGC 2516 (Briggs & Pye 2003; Pillitteri et al. 2004). The ratio of hot to cool emission measures in 2-T models suggests that the two thermal components are comparable, the ratio being between 0.5 and 3.0 with a median of 1.3.

Spectra of all but 3 early type stars ($B - V \lesssim 0.5$) have low count statistics: we may obtain a good fit of them with 1-T models. In this case the temperatures lie around 0.6 keV,

suggesting that the spectra are softer than those of solar mass stars.

The star DK 56 (a binary system with a B2V star and an unresolved late type companion) was bright enough in each observation to fit its spectrum with a 2-T model. We found a hot spectrum with temperatures of 0.8 and 3.0 keV and a spectrum shape similar to those of solar type stars. In the case of a wind driven X-ray emission, typical of massive stars, the spectrum is expected to be softer than in the case of coronae of solar mass stars. Therefore, based on the spectrum shape and temperatures, we suggest that the X-ray emission of DK 56 is likely due to or strongly affected by the late type companion. This is a conclusion opposite to that of Jeffries et al. (1997) who, on the basis of its high X-ray luminosity, attributed all the X-ray emission of DK56 to the massive primary. This system is a blue straggler of the cluster, younger than ∼25 Myr (Dachs & Kabus 1989). Based on this age estimate, these authors discussed the hypothesis of subsequent episodes of star formation in NGC 2516 determined by the crossing of the cluster through the Galactic Plane or the Gum Nebula. Given this age estimate, the high X-ray luminosity of the order of 10^{30} erg s^{-1} is not an atypical value for solar-type stars of 25 Myr or less.

3.3. The X-ray luminosities of NGC 2516 late type stars

We have calculated the Kaplan-Meier estimators (Feigelson & Nelson 1985) of the distribution of X-ray luminosities for F, G, K and M spectral types. The distributions take into account the the upper limits in $\log L_X$ that censorize the sample. When the lowest values are upper limits the distribution does not reach unity. Figure 6 shows the X-ray distribution functions for F-, G-, K- and M-type stars of NGC 2516 (solid lines); for comparison we have added the ROSAT data of Pleiades (Micela et al. 1999, dotted line) and the distribution considering only detections of NGC 2516 (solid gray line). This is an upper bound to the true distribution which must include undetected members. The Kaplan-Meier estimators of Pleiades and NGC 2516 are different[2]. In particular, the luminosities of NGC 2516 of G-, K- and M- type stars are systematically lower than those of the Pleiades, the difference being larger for G- and K-type stars where the contamination of the optical catalog is higher than in the other spectral ranges, as stated by Jeffries et al. (2001). Especially among K-type stars the Kaplan-Meier estimator and cumulative distribution of X-ray detections alone show the largest difference.

The contamination by less active field stars among G- and K-type stars in NGC 2516 hampers the evaluation of L_X distributions of NGC 2516. However, the X-ray luminosities of detections alone of G-, K- and M-type stars are systematically lower than the luminosities of the Pleiades at a level ≥99% as obtained by applying several two sample tests. The distribution of detections alone shown in Fig. 6 may be interpreted as an upper limit for the *true* cumulative distribution of X-ray luminosity. If we were able to take into account the upper limits of

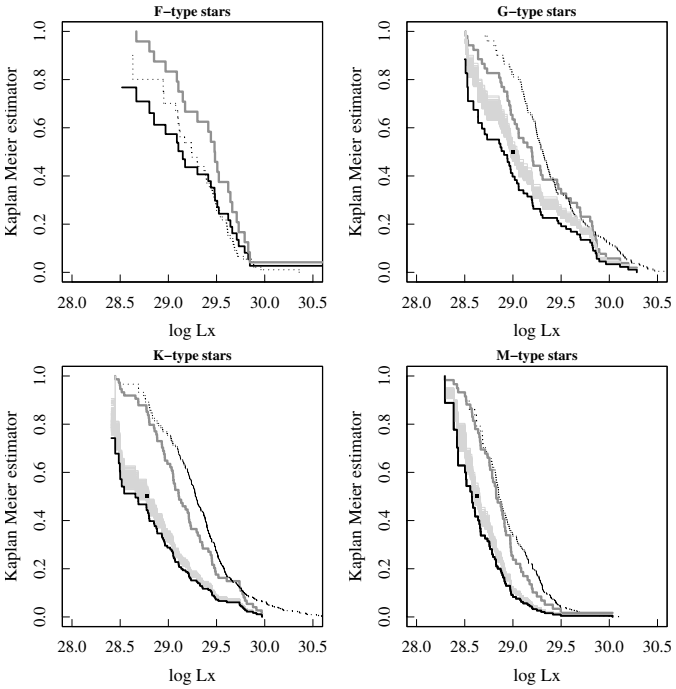

Fig. 6. Cumulative distribution functions of X-ray luminosities of NGC 2516 stars (solid black line) with different spectral types, evaluated with Kaplan Meyer estimators. Dotted lines are the distributions of Pleiades (Micela et al. 1999). Solid gray lines in G-, K- and M-type stars are the distribution of detections alone. The gray area in G-, K- and M-type panels marks the envelop of simulated Kaplan-Meier estimators after statistical correction for contaminants; the black square inside each area is the average of their medians.

only *true* cluster members, the Kaplan-Meier estimators should be at lower luminosities with respect to the distribution of detections alone.

We have evaluated how many field stars are expected to fall among our X-ray detections. We focused on the main sequence field stars expected to be in a volume determined by the photometric selection of the cluster Main Sequence and the sky area of our survey. By using the stellar density given in Cox (2000), Table 19.14 (valid for stellar density on the galactic plane, NGC 2516 is ∼100 pc above the Galactic Plane) we estimated 11 and 19 G and K-type main sequence field stars in that volume and not related to the cluster.

From the X-ray luminosity distributions reported in Schmitt et al. (1995) and Schmitt (1997) G-type field stars have $\log L_X/(\mathrm{erg\,s^{-1}})$ in the range 26.5–29.5 with median 27.3; K-type stars occupy a narrower range (27.1–28.4) with a median of $\log L_X/(\mathrm{erg\,s^{-1}}) = 27.6$. M-type stars in the solar neighborhood have luminosities $25.5 \leq \log L_X/(\mathrm{erg\ s^{-1}}) \leq 29.1$ and a median of $\log L_X/(\mathrm{erg\ s^{-1}}) \sim 27$. Hence we estimated that less than 3 field stars in each spectral type should have been detected among the photometric sample (at the same time a sample of 10 to 18 stars should be undetected in the surveyed volume). More distant giants should not be detected and thus they should not affect the distribution of detections alone. The expected field star detections are thus very few compared to the number of detected cluster members in each sample

[2] By applying several two sample tests, the difference between the two curves is significant at a level ≥99.9%.

(52 G-, 74 K- and 59 M-type detections), thus the distribution of detections alone should not be affected by field stars.

We have taken into account the expected fraction of contaminants given by Jeffries et al. (2001) in order to estimate *unbiased* X-ray luminosity distribution functions of NGC 2516 G-, K- and M-type stars. By following the method used in Damiani et al. (2003), we excluded a fraction of upper limits from the X-ray luminosity sample in each spectral type according to the membership probability and assuming that the contaminants yield only upper limits; then we calculated the Kaplan-Meier estimator. This simulation procedure was iterated 500 times producing thus the bunch of curves plotted in light gray in Fig. 6 and which define the region where the *true* distribution function should lie. Only in the case of G-type stars do we observe a larger difference between the curve with upper limits and the family of contaminant corrected curves. In the K- and M-type stars the large number of upper limits is less affected by the statistical correction for contaminants. In all cases the gray region is at lower X-ray luminosities than the Pleiades cumulative distributions.

The averages of the 0.5 quantile of each simulated curve are marked in each panel with a black square; the $\log L_X/(\mathrm{erg\ s^{-1}})$ values are 29.04, 28.82 and 28.68 for G-, K- and M-type stars, respectively; the width of the gray region at the 0.5 quantile is ∼0.05 dex which we assume as the uncertainty on the previous averages. Güdel (2004) and Favata & Micela (2003) discuss X-ray emission as a function of age for stars from young stellar objects to aged open clusters and the Sun. We have plotted in Fig. 7 the medians of $\log L_X$ for F-, G-, K- and M-type stars reported by Güdel (2004) and our $\log L_X$ medians (after contaminant correction) for the same spectral types as a function of age. We have assumed here an age of 140 Myr for NGC 2516. We see a decrease of the mean level of X-ray luminosities with age, after a plateau at $\sim 10^{30}$ erg s^{-1} which extends from Orion and Taurus Star forming Region ages (few Myr) to Alpha Persei cluster age (50 Myr). The X-ray under-luminosity of NGC 2516 with respect to the nearly coeval Pleiades remains evident, even taking into account the statistical correction for non member contamination and any systematic uncertainty discussed in Sect. 2.2.

The causes of the different levels of luminosity of solar type stars in NGC 2516 and the Pleiades could be attributed to several factors. Rotation is a key parameter for X-ray emission (Pallavicini et al. 1981) up to rotations as fast as $v \sin i \sim 20$ km s^{-1}, when the L_X – rotation relation flattens. Furthermore, angular momentum losses due to magnetic braking link stellar rotation to age and X-ray activity. A different distribution of rotation rates in the Pleiades and NGC 2516 could explain the low X-ray luminosity observed in the latter cluster. Jeffries et al. (1998) studied the stellar rotation of solar type stars of NGC 2516, finding a lower rotational rate in F- early and G- type stars with respect to the Pleiades whereas no clear difference between these two clusters was found among K-type stars. However Terndrup et al. (2002) concluded that no significant difference in rotation distribution is present between the Pleiades and NGC 2516, if this latter is assumed slight older than Pleiades. The under-luminosity of NGC 2516 in X-rays seems to arise essentialy from the slight

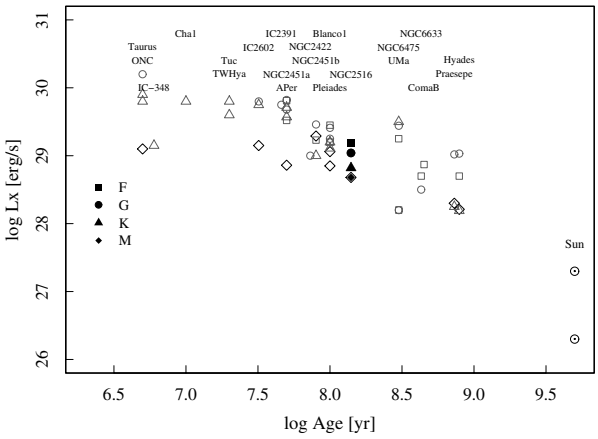

Fig. 7. $\log L_X$ vs. age for different open clusters, star forming regions and the Sun. Open symbols: data of all but NGC 2516 clusters from Güdel (2004); solid symbols: medians of NGC 2516 F-, G-, K- and M-type stars (contaminants corrected, see. Sect. 3.3) from the present work.

difference of age between the two clusters (80–100 Myr for Pleiades, 140 Myr for NGC 2516), although the past history of NGC 2516, its location and kinematics could have played a role in determining peculiar forming conditions, perhaps different to those of the Pleiades with an influence on the X-ray emission evolution.

3.4. L_X to L_{bol} ratio

An indicator of activity is the ratio of X-ray to stellar bolometric luminosity, $\log L_X/L_{bol}$. Because of the dependence of X-ray luminosity on rotation, the $\log L_X/L_{bol}$ ratio follows a power law relation of index –2 with rotational period and the Rossby number, i.e. the ratio between rotational period and convective turnover time in *non saturated* stars (see Patten & Simon 1996; Randich 2000; Pizzolato et al. 2003). ROSAT observations of young open clusters in the band 0.1–2.4 keV have also shown that low mass stars exhibit a saturation of this ratio at the level of ∼–3, i.e. the X-ray luminosity reaches at most 1/1000 of bolometric luminosity of the star. Furthermore, saturation seems to occur at earlier types in younger stars ($B - V = 0.7$ or late G-type stars at the age of the Pleiades, $B - V = 1$ or mid K-type stars at 220 Myr, Prosser et al. 1995).

We calculated the bolometric luminosities of NGC 2516 by interpolating L_{bol} as a function of $(B-V)$ based on an isochrone model with $Z = 0.02$ and age of 140 Myr (Siess et al. 2000); for stars with $(B - V)_0 \geq 0.3$ we used $(V - I)$ color instead of $(B - V)$. Figure 8 shows $\log L_X/L_{bol}$ of NGC 2516 stars versus their $B - V_0$ and $V - I_0$ colors, with open and filled circles for single and binaries, respectively. We did not correct L_{bol} for unresolved binary systems. These unresolved binaries trace an upper sequence in the plots. Arrows represent upper limits and the bottom curve approximately traces the detection limit at the cluster distance ($\log L_X \sim 28.4$). A spread of ∼1.4 dex is observed among detections in $0 \leq B - V \leq 1.5$ where $\log L_X/L_{bol}$ may reach values up to –2.4. The highest point at ∼–1.4 is due to a very cool star ($V - I = 3.06$, id. 6160 in the Jeffries et al. 2001 catalog): however this star is very close to the edge of the

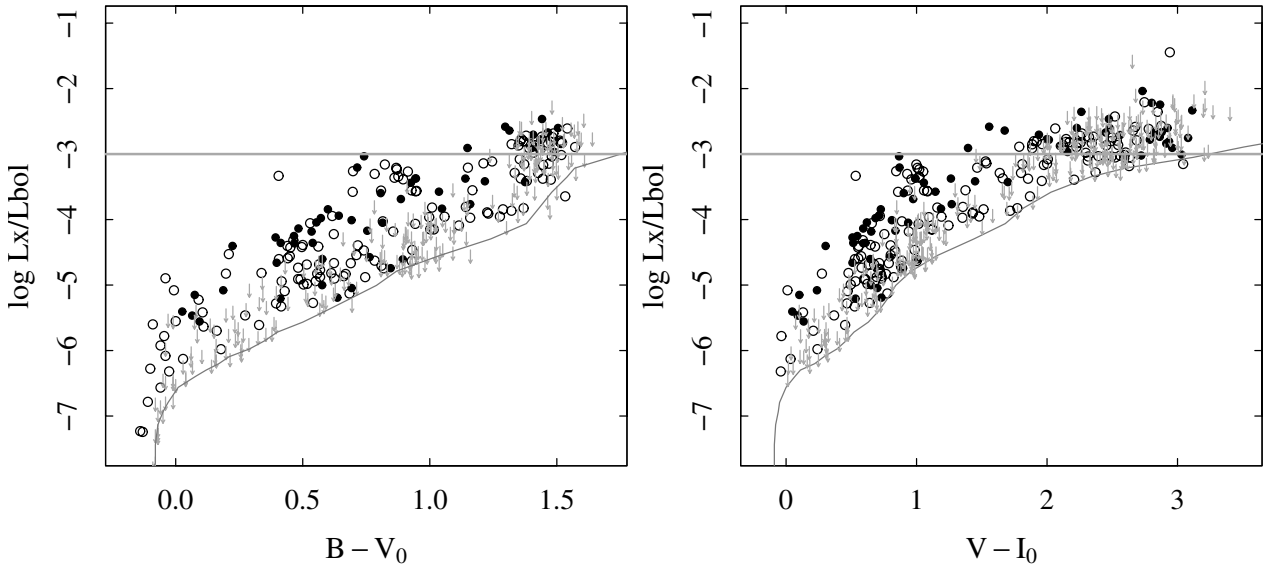

Fig. 8. Logarithmic X-ray to bolometric luminosity ratio of NGC 2516 stars. Open circles: detected single stars, filled circles: detected binaries, vertical arrows: upper limits. Lines below data points roughly trace the detection limit at the cluster distance ($\log L_X \sim 28.4$).

field of view and was observed only during the first observation, hence its X-ray luminosity is quite uncertain.

The $\log L_X/L_{bol}$ ratio flattens at $(V-I)_0 \sim 1.5$ or $(B-V)_0 \sim 0.7$, which corresponds to the spectral type K5, according to the color-temperature calibration by Kenyon & Hartmann (1995) and we observe a saturation value of $\log L_X/L_{bol} \sim -2.5$ instead of –3. A comparison with L_{bol} used by Jeffries et al. (1997) shows that our L_{bol} are on average lower by 0.1 dex for stars detected in both surveys. This difference would produce a shift toward high $\log L_X/L_{bol}$ ratio, while the trend and the spectral type at which the saturation of $\log L_X/L_{bol}$ occurs should not be changed.

4. Comparison with Chandra and ROSAT surveys

NGC 2516 has been observed several times with the *Chandra* satellite between August 1999 and March 2001 with different instrument setups; a deep survey was obtained by Damiani et al. (2003) combining several exposures from ACIS and HRC cameras. In that work 155 cluster stars were detected in X-ray while 570 remained undetected. There are 535 stars falling both in the XMM-Newton and Chandra fields of view; out of this sample we have detected 125 stars with the EPIC camera also detected with Chandra; a further 100 stars are detected with EPIC whereas they were undetected in Chandra images. Only 17 stars are detected with Chandra but not with XMM-Newton; 293 stars remain undetected in both surveys. In Fig. 9 we show the comparison of Chandra and XMM-Newton X-ray luminosities for the stars detected in at least one of these surveys. The plot shows that a scatter of a factor $\lesssim 2$ is observed in most cases; sometimes a difference of a factor 5 or more may be present also in a few massive stars (DK 55 / HD 66167, B9.5V + A0V; HD 66194 / DK 56, sp. type B2IV).

The upper limits marked by arrows in the lower right corner of Fig. 9 are stars undetected with Chandra but detected with XMM-Newton. This large number of upper limits is due to the sensitivity of our survey being a factor of ∼5 higher than the Chandra one. The maximum sensitivity is comparable in both satellite instruments but in Chandra the decrease of sensitivity at large off-axis angles is more marked. Both the large effective area of XMM-Newton telescopes and the more uniform point spread function (PSF) throughout the EPIC field of view result in a higher efficiency of the EPIC camera in detecting off-axis sources (thus in a larger sky area) than ACIS and HRC detectors. Chandra has a higher spatial resolution near the center of the field of view, but its PSF profile rapidly degrades at increasing off-axis angles thus reducing the efficiency in detecting faint sources.

The Sun activity is characterized by the 11-yr cycle. The maximum variation of amplitudes in the Sun cycle is a factor greater than 20. In order to study the time variability on time scales of about 12 years we have compared the X-ray luminosities of NGC 2516 stars falling in the field of view of ROSAT observations taken in 1993 and analyzed by Jeffries et al. (1997). This time scale should allow us to detect stellar cycles present in NGC 2516 stars with amplitudes and periods similar to those observed on the Sun. Figure 10 shows the X-ray luminosities measured with XMM-Newton and with ROSAT; XMM-Newton luminosities were recalculated coherently in the ROSAT band. Error bars for both XMM and ROSAT L_X are plotted, the latter obtained from Jeffries et al. (1997). The lowest L_X detected with ROSAT is $\sim 10^{29}$ erg/s. Only two stars detected in both surveys, JTH 9465 (also JTX 138 in SIMBAD) and JTH 10817 (JTX 114), changed luminosity by a factor between 2 and 5, due to flare variability during one of the six XMM-Newton observations. The variability of these two stars is discussed in Ramsay et al. (2003). Another four stars (JTH 10863, 10871, 12649 and 15514), undetected by ROSAT, are interesting because they are variable in the XMM survey by more than a factor of two with respect to their ROSAT upper limits. Most of the stars have variations within a factor of two. The modest variability on long time scales has been

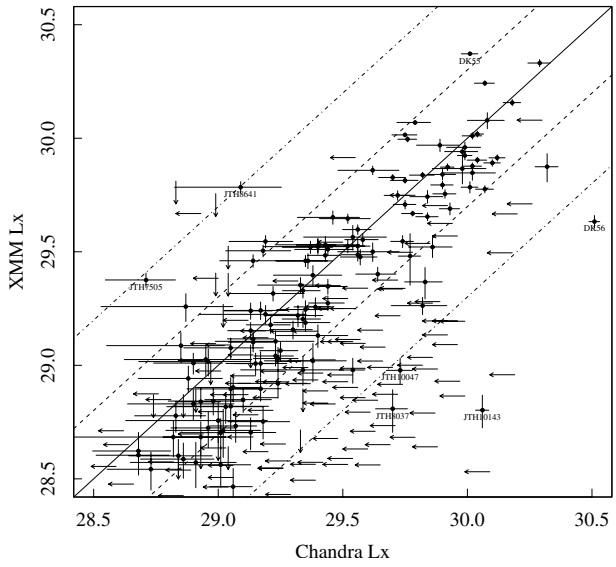

Fig. 9. XMM-Newton vs. Chandra (Damiani et al. 2003) measurements of X-ray luminosities of NGC 2516 stars detected at least once in the two surveys. Error bars are the statistical uncertainties; the horizontal arrows mark upper limits for undetected stars in Chandra, while vertical ones refer to XMM-Newton undetected stars. Solid, dashed and dot-dashed lines trace the equal, two and five times (and their reciprocal) ratios. We indicate the names of a few stars with large variability, JTH are from Jeffries et al. (2001), while DK refers to Dachs & Kabus (1989).

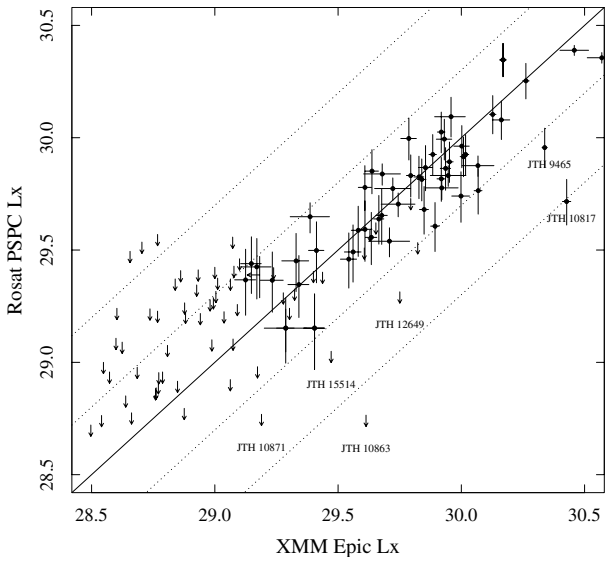

Fig. 10. X-ray luminosities of XMM detected stars of NGC 2516 compared with values obtained with ROSAT satellite by Jeffries et al. (1997). Arrows mark upper limits due to ROSAT undetected stars. The continuous line and dotted lines correspond to 1, 1/5, 1/2, 2 and 5 ratio between XMM-Newton and ROSAT luminosities, respectively.

reported by Wolk et al. (2004), in a study of X-ray time variability of NGC 2516 based on Chandra data. These variations are smaller than expected in the presence of solar cycles and strongly suggest that cycles in young stars are absent or have different periods and/or smaller amplitudes than those observed in the Sun.

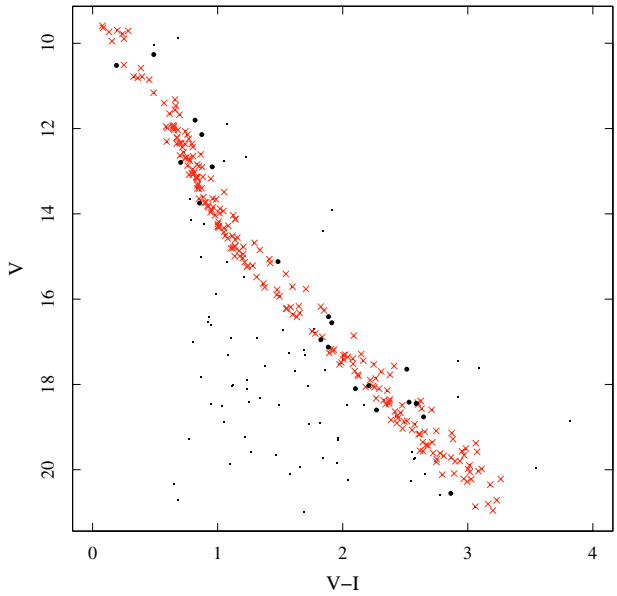

Fig. 11. Color–magnitude diagram of X-ray sources matching the optical catalog of Jeffries et al. (2001). Small dots: all sources, crosses: NGC 2516 stars, large dots: suggested new cluster members.

5. New possible members and unidentified sources

A number of X-ray detections have optical photometry consistent with the membership of NGC 2516. On this basis these stars could be cluster members. Figure 11 shows the color–magnitude diagram of the X-ray sources from the Jeffries catalog. By placing them at the cluster distance, their X-ray luminosities range between 3.7×10^{28} and 1.5×10^{30} erg/s. In Table 4 we list the main properties of these objects.

A few X-ray sources do not have counterparts in optical or infrared bands. After having searched for optical counterparts of the X-ray sources in GSC-II, 2MASS and DENIS and the complete catalog of Jeffries et al. (2001), 49 sources are left without optical/infrared known counterparts. We have marked these sources with a U in the last column of Table A.1: the finding charts at their positions are reported in Figs. D.1 and D.2.

6. Summary

We have presented results from a deep X-ray survey of the young open cluster NGC 2516, obtained from a series of six XMM-Newton observations. The source detection has been carried out on the sum of EPIC MOS and pn images with a wavelet transform code (PWXDetect). We have reached fluxes lower by a factor of 5 or more than Chandra observations carried out in the same epoch. We have detected 431 sources, 234 of them have as optical counterparts 239 cluster members, five X-ray sources match as many close pairs. X-ray emission of spectral type from early B down to M-type stars has been detected; the coolest detected stars have spectral type M5 and $T_{\rm eff} \sim 3000$. We have investigated the X-ray spectral properties of cluster stars through 1-T and 2-T models to estimate the dominant plasma thermal components and emission measures. For 1-T models we find temperatures around

Table 4. Properties of new suggested cluster members. Columns are: id. number in Jeffries et al. (2001) catalog, X-ray source number as in Table A.1, V, $B-V$, $V-I$, match distance between X and optical position, flux and X-ray luminosity in 0.3–7.9 keV, calculated by assuming them as cluster members.

Opt id JTH#	X Src	V mag	$B-V$ mag	$V-I$ mag	r $''$	log f_X erg s^{-1} cm^{-2}	log L_X erg s^{-1}
5337	22	16.412	1.288	1.887	0.8	–13.44	29.81
7417	53	18.418	1.276	2.53	0.9	–13.96	29.29
6220	67	15.123	1.177	1.481	0.9	–13.39	29.87
9976	72	17.123	1.312	1.884	0.6	–14.04	29.21
7485	75	11.801	0.771	0.819	1.1	–13.97	29.28
9022	76	18.448	1.74	2.587	1.6	–14.08	29.18
8692	88	18.029	1.379	2.208	0.8	–14.68	28.57
7200	93	18.599	–	2.27	2.2	–14.48	28.78
7708	110	17.643	1.714	2.512	2.8	–13.84	29.41
5447	167	16.555	1.348	1.912	1.5	–13.76	29.5
7129	170	18.098	–	2.101	0.2	–14.06	29.19
7147	217	13.747	0.726	0.856	0.7	–13.55	29.7
9492	243	10.518	0.148	0.191	1.6	–14.69	28.57
11455	264	18.759	1.348	2.646	1.5	–14.64	28.61
11366	292	12.898	0.827	0.956	2.2	–13.07	30.18
7844	324	12.14	0.368	0.873	2	–14.05	29.21
9106	341	10.262	0.405	0.49	1.8	–14.49	28.76
9467	348	16.95	1.132	1.825	0.3	–14.21	29.04
4181	352	20.553	–	2.865	2.6	–13.45	29.8
6700	413	12.792	0.597	0.704	2.2	–14.08	29.17

0.6 keV. In 2-T models the temperatures are in 0.3–0.7 keV and 1.0–2.0 keV ranges in agreement with the temperatures found in nearly coeval open clusters like Pleiades and Blanco 1.

For each spectral type F, G, K, M we estimated the maximum likelihood distribution of X-ray luminosities taking also into account the upper limits for undetected cluster stars. G-, K-, and M- type stars are under-luminous with respect to the Pleiades in the same spectral range. Possible biases due to contaminating field stars are discussed and statistical corrections have been made to X-ray distribution functions. We conclude that the NGC 2516 solar type stars are definitively less luminous in X-rays than the analog Pleiades. The differences could be attributed mainly to the slight older age of NGC 2516 (140 Myr vs. 80–100 Myr of Pleiades), less probably to a lower rotation rate. The past cluster history could also have a role in determining X-ray emission.

By comparing XMM-EPIC and ROSAT-PSPC data we explored X-ray variability on time scales comparable to the solar cycle. We observe only variations in X-ray luminosities by a factor of 2–3. Along with what is seen in other coeval open clusters, this result strongly suggests that activity cycles of amplitude and periods like the solar one are not present in young Main Sequence stars at an age of ∼140 Myr.

We identify 20 likely new candidate members on the basis of their X-ray emission and optical photometry. 49 X-ray sources are left unidentified in optical and infrared bands and are likely of extragalactic nature and for them we provide finding charts.

Acknowledgements. Authors acknowledge financial support from MIUR-PR/N grant (Ministero dell'Istruzione, Università e Ricerca).

References

Babel, J., & Montmerle, T. 1997, ApJ, 485, L29
Briggs, K. R., & Pye, J. P. 2003, MNRAS, 345, 714
Cassinelli, J. P., & MacGregor, K. B. 2000, in ASP Conf. Ser., 337
Cox, A. N. 2000, Allen's astrophysical quantities, Allen's astrophysical quantities, ed. A. N. Cox, 4th ed. (New York: AIP Press; Springer)
Dachs, J. 1970, A&A, 5, 312
Dachs, J., & Kabus, H. 1989, A&AS, 78, 25
Damiani, F., Flaccomio, E., Micela, G., et al. 2003, ApJ, 588, 1009
Damiani, F., Maggio, A., Micela, G., & Sciortino, S. 1997a, ApJ, 483, 350
Damiani, F., Maggio, A., Micela, G., & Sciortino, S. 1997b, ApJ, 483, 370
Favata, F., & Micela, G. 2003, Space Sci. Rev., 108, 577
Feigelson, E. D., & Nelson, P. I. 1985, ApJ, 293, 192
Feldmeier, A. 1995, A&A, 299, 523
Gondoin, P. 2005, A&A, 438, 291
Güdel, M. 2004, A&AR, 12, 71
Harnden, F. R., Adams, N. R., Damiani, F., et al. 2001, ApJ, 547, L141
Jeffries, R. D., James, D. J., & Thurston, M. R. 1998, MNRAS, 300, 550
Jeffries, R. D., Thurston, M. R., & Hambly, N. C. 2001, A&A, 375, 863
Jeffries, R. D., Thurston, M. R., & Pye, J. P. 1997, MNRAS, 287, 350
Kenyon, S. J., & Hartmann, L. 1995, ApJS, 101, 117
Lucy, L. B., & White, R. L. 1980, ApJ, 241, 300

Marino, A., Micela, G., Peres, G., Pillitteri, I., & Sciortino, S. 2004, A&A, in press
Meynet, G., Mermilliod, J.-C., & Maeder, A. 1993, A&AS, 98, 477
Micela, G., Sciortino, S., Harnden, et al. 1999, A&A, 341, 751
Micela, G., Sciortino, S., Jeffries, R. D., Thurston, M. R., & Favata, F. 2000, A&A, 357, 909
Pallavicini, R., Golub, L., Rosner, R., et al. 1981, ApJ, 248, 279
Patten, B. M., & Simon, T. 1996, ApJS, 106, 489
Pillitteri, I., Micela, G., Sciortino, S., Damiani, F., & Harnden, F. R. 2004, A&A, 421, 175
Pizzolato, N., Maggio, A., Micela, G., Sciortino, S., & Ventura, P. 2003, A&A, 397, 147
Prosser, C. F., Stauffer, J. R., Caillault, J.-P., et al. 1995, AJ, 110, 1229
Ramsay, G., Harra, L., & Kay, H. 2003, MNRAS, 341, 1388
Randich, S. 2000, in Stellar Clusters and Associations: Convection, Rotation, and Dynamos, ASP Conf. Ser., 198, 401
Rauw, G., De Becker, M., Gosset, E., Pittard, J. M., & Stevens, I. R. 2003, A&A, 407, 925
Schmitt, J. H. M. M. 1997, A&A, 318, 215
Schmitt, J. H. M. M., Fleming, T. A., & Giampapa, M. S. 1995, ApJ, 450, 392
Sciortino, S., Micela, G., Damiani, F., et al. 2001, A&A, 365, L259
Siess, L., Dufour, E., & Forestini, M. 2000, A&A, 358, 593
Terndrup, D. M., Pinsonneault, M., Jeffries, R. D., et al. 2002, ApJ, 576, 950
Vaiana, G. S., Fabbiano, G., Giacconi, R., et al. 1981, ApJ, 245, 163
van den Berg, M., Tagliaferri, G., Belloni, T., & Verbunt, F. 2004, A&A, 418, 509
Waldron, W. L., & Cassinelli, J. P. 2001, ApJ, 548, L45
Wolk, S. J., Harnden, F. R., Murray, S. S., et al. 2004, ApJ, 606, 466

Online Material

Appendix A: X-ray detections

Table A.1. List of detected X-ray sources in the combined images of the XMM-Newton EPIC camera. Columns report: running number of X-ray detection, coordinates, count rate in MOS1 equivalent counts, detection significance (in units of background mean standard deviation), total exposure time, offaxis distance and unidentified source flag (cf. Sect. 4).

Num	RA J2000	Dec J2000	Count rate cts ks^{-1}	Signif.	Exp. time ks	Offaxis arcmin	Un.
1	07:57:20.63	–61:4:19.27	4.38 ± 0.82	10.74	8	18.46	
4	07:58:23.5	–61:3:44.57	1.49 ± 0.27	7.59	49.55	16.56	
6	07:57:17.67	–61:3:30.6	7.05 ± 0.75	14.34	16.66	17.85	
7	07:57:40.35	–61:3:31	0.62 ± 0.16	5.81	46.76	16.93	
8	07:58:34.76	–61:3:17.86	1.93 ± 0.29	9.28	50.52	16.23	
9	07:57:47.6	–61:3:6.98	0.84 ± 0.17	7.21	50.04	16.32	
10	07:58:26.91	–61:2:46.14	1.16 ± 0.21	8.07	54.34	15.61	
11	07:58:44.52	–61:2:37.93	0.68 ± 0.2	5.66	28.18	15.78	
12	07:57:38.58	–61:2:10.9	4.83 ± 0.4	21.14	49.11	15.71	
13	07:58:12.85	–61:2:10.28	2.82 ± 0.3	14.41	57.71	14.98	U
15	07:57:35.79	–61:2:6.54	0.73 ± 0.2	6.16	29.76	15.74	
16	07:57:57.76	–61:2:5.06	1.04 ± 0.19	7.2	56.76	15.07	
18	07:58:43.13	–61:1:59.66	2.51 ± 0.29	14.52	49.01	15.12	U
19	07:59:28.83	–61:1:58.01	1.06 ± 0.24	6.21	38.19	17.13	
20	07:57:10.68	–61:1:27.34	1.22 ± 0.27	5.47	46.06	16.4	
21	07:57:56.85	–61:0:58.75	1.73 ± 0.2	13.38	68.94	14	
22	07:56:56.25	–61:0:57.17	3.79 ± 0.77	7.24	10.86	16.93	
23	07:59:36.78	–61:0:57.02	1.22 ± 0.24	7.13	41.21	16.8	U
24	07:58:53.92	–61:0:24.48	0.9 ± 0.15	8.55	75.47	13.93	
25	07:57:43.44	–61:0:0.79	0.99 ± 0.16	8.38	68.58	13.46	
27	07:58:3.12	–60:59:56.29	1.62 ± 0.18	15.07	85.46	12.85	
29	07:58:32.24	–60:59:48.62	1.07 ± 0.15	10.28	108.33	12.74	
30	07:57:8.39	–60:59:45.06	1.24 ± 0.24	6.62	51.24	15.1	
31	07:58:9.17	–60:59:42.36	0.39 ± 0.08	6.72	111.72	12.54	
32	07:57:31.49	–60:59:30.8	4.87 ± 0.35	28.3	61.47	13.52	
34	07:58:22.4	–60:59:9.02	0.31 ± 0.06	6.56	121.29	11.96	
35	07:58:35.72	–60:59:2.62	0.55 ± 0.1	7.84	133.7	12.05	U
36	07:56:38.76	–60:58:58.84	1.84 ± 0.39	6.36	16.43	16.82	
37	07:57:7.52	–60:58:55.7	0.66 ± 0.17	6.19	43.66	14.48	U
38	07:58:21.47	–60:58:52.1	1.46 ± 0.15	13.52	139.39	11.68	
39	07:59:32.14	–60:58:47.89	2.16 ± 0.27	12.41	50.32	14.73	
40	07:58:11.66	–60:58:38.14	0.74 ± 0.1	10.85	146.54	11.46	U
41	07:58:6.65	–60:58:34.18	0.38 ± 0.08	6.2	146.23	11.44	
42	07:59:25.06	–60:58:30.29	5.36 ± 0.36	26	69.39	13.98	U
43	07:58:31.7	–60:58:28.13	0.41 ± 0.09	6.17	138.94	11.4	
44	07:57:53.41	–60:58:22.01	4.82 ± 0.24	35.53	133	11.54	
45	07:58:51.45	–60:58:15.78	0.69 ± 0.1	9.58	135.04	11.81	
46	07:56:55	–60:58:13.76	1.12 ± 0.2	9.38	49.13	14.91	
47	07:57:27.7	–60:58:13.51	1.02 ± 0.21	7.05	59.56	12.57	
48	07:59:5.46	–60:58:9.3	0.75 ± 0.11	9.42	118.15	12.42	
49	07:57:21.21	–60:58:4.08	0.81 ± 0.16	6.71	65.03	12.84	U
50	07:59:32.98	–60:57:58.25	1.03 ± 0.18	8.2	66.45	14.16	U
51	07:58:20.05	–60:57:54.54	0.65 ± 0.1	9.52	134.22	10.71	U
53	07:57:51.12	–60:57:29.59	1.15 ± 0.12	12.6	152.69	10.78	
55	07:56:34.67	–60:57:25.31	1.79 ± 0.33	10.19	17.21	16.15	
56	07:57:31.24	–60:57:27.14	0.72 ± 0.14	6.58	108.83	11.69	U
57	07:58:52.02	–60:57:26.57	0.75 ± 0.1	11.02	134.6	11.07	
58	07:57:7.35	–60:57:5.22	1.16 ± 0.2	7.24	65.92	13.06	
59	07:59:8.48	–60:57:3.49	0.64 ± 0.11	9.36	139.69	11.65	
60	07:57:59.19	–60:56:53.95	5.67 ± 0.21	55.7	177.01	9.95	
61	07:57:25.25	–60:56:50.57	1.85 ± 0.18	14.23	83.85	11.54	
62	07:58:49.72	–60:56:50.86	0.29 ± 0.06	6.48	176.33	10.42	U
63	07:56:47.55	–60:56:48.3	7.04 ± 0.57	20.41	31.91	14.56	
64	07:59:9.25	–60:56:39.91	1.02 ± 0.12	12.65	144.98	11.37	
65	07:58:53.66	–60:56:34.04	0.97 ± 0.1	15.55	179.67	10.35	
66	07:58:58.09	–60:56:33.22	0.36 ± 0.07	6.57	177.39	10.58	

Table A.1. continued.

Num	RA J2000	Dec J2000	Count rate cts ks^{-1}	Signif.	Exp. time ks	Offaxis arcmin	Un.
67	07:57:19.36	–60:56:29.11	4.32 ± 0.23	35.57	119.41	11.67	
68	07:57:45.01	–60:56:20.29	0.3 ± 0.07	6.11	179.71	9.95	
69	07:57:47.54	–60:56:19.28	0.72 ± 0.1	9.08	176.81	9.82	
70	07:57:30.2	–60:56:16.01	0.4 ± 0.08	6.28	144.77	10.73	
71	07:58:50.67	–60:56:3.77	1.15 ± 0.1	17.04	191.13	9.74	U
72	07:58:55.42	–60:55:59.63	0.95 ± 0.1	14.62	179.62	9.93	
73	07:59:34.23	–60:55:53.22	2.21 ± 0.18	16.91	118.09	12.76	
74	07:57:26.72	–60:55:49.8	0.32 ± 0.07	5.58	165.11	10.61	
75	07:57:52.91	–60:55:45.12	1.12 ± 0.09	18.95	200.44	9.06	
76	07:58:32.68	–60:55:44.33	0.88 ± 0.1	12.42	210.36	8.74	
77	07:57:20.65	–60:55:43.07	1.39 ± 0.13	14.44	158.56	10.97	
78	07:58:48.6	–60:55:25.93	0.61 ± 0.08	10.86	202.74	9.06	
79	07:58:43.22	–60:55:25.82	10.55 ± 0.26	94.66	208.29	8.81	
80	07:59:23.15	–60:55:13.22	0.33 ± 0.06	7.52	160.1	11.33	
81	07:58:18.23	–60:55:10.06	0.3 ± 0.05	8.56	215.57	7.97	
84	07:57:56.18	–60:54:58.57	1.32 ± 0.11	18.02	212.38	8.19	
85	07:58:23.35	–60:54:58.18	7.15 ± 0.2	78.44	225.84	7.8	
86	07:57:57.2	–60:54:56.02	0.18 ± 0.04	8.38	215.99	8.11	
87	07:58:16.68	–60:54:52.56	0.28 ± 0.05	8.36	226.1	7.67	
88	07:58:24.46	–60:54:40.68	0.22 ± 0.05	8.26	229.69	7.53	
89	07:57:37.8	–60:54:33.19	2.55 ± 0.14	33.85	198.47	8.79	
90	07:58:53.58	–60:54:25.74	1.48 ± 0.11	23.87	210.34	8.46	
91	07:58:27.26	–60:54:24.84	0.2 ± 0.05	5.07	216.35	7.31	U
92	07:57:54.42	–60:54:22.75	0.18 ± 0.04	5.69	221.64	7.7	
93	07:57:45.08	–60:54:18	0.35 ± 0.06	7.25	209.26	8.12	
94	07:58:47.85	–60:54:15.62	6.5 ± 0.2	69.17	220.94	7.97	
95	07:58:18.51	–60:54:15.77	0.26 ± 0.05	6.52	230.77	7.06	
96	07:56:47.45	–60:54:12.06	2 ± 0.22	16.19	65.93	13	
97	08:00:2.25	–60:53:54.31	1.28 ± 0.2	11.02	56.36	14.42	
98	07:57:24.59	–60:53:54.42	0.21 ± 0.05	5.38	183.08	9.29	
99	07:58:31.93	–60:53:52.87	1.22 ± 0.09	22.46	240.29	6.91	
100	07:56:59.9	–60:53:47.76	0.77 ± 0.11	9.57	127.24	11.52	
102	07:57:21.46	–60:53:43.48	0.57 ± 0.1	7.29	160.85	9.43	
103	07:57:57.67	–60:53:40.52	4.02 ± 0.16	45.13	227.04	6.91	
104	07:58:52.29	–60:53:38.83	2.3 ± 0.12	35.31	222.43	7.72	
105	07:58:31.57	–60:53:11.65	2.09 ± 0.11	36.48	247.59	6.24	
106	07:57:47	–60:53:9.02	0.51 ± 0.08	8.09	226.47	7.01	U
107	07:57:15.49	–60:53:2.47	0.47 ± 0.08	8.17	165.29	9.54	
108	07:57:55.2	–60:52:58.66	0.18 ± 0.04	7.15	241.77	6.38	
109	07:58:41.92	–60:52:55.81	0.53 ± 0.08	7.62	224.36	6.46	
110	07:57:57.96	–60:52:48.72	1.52 ± 0.1	25.24	220.39	6.09	
111	07:58:4.58	–60:52:44.22	0.65 ± 0.07	14.01	249.66	5.75	
112	08:00:13.26	–60:52:40.44	2.85 ± 0.35	12.23	50.02	15.14	
113	07:59:3.77	–60:52:35.58	1.57 ± 0.11	27.54	209.1	7.81	U
114	07:57:41.17	–60:52:31.66	0.78 ± 0.09	11.82	219	6.92	
115	07:57:30.37	–60:52:29.68	0.21 ± 0.05	6.76	182.97	7.8	
116	07:58:31.33	–60:52:25.64	0.25 ± 0.04	8.64	239.62	5.49	
117	07:59:20.41	–60:52:22.37	0.64 ± 0.09	8.49	183.63	9.26	
118	07:58:48.46	–60:52:21.83	2.79 ± 0.13	36.22	244.64	6.4	
119	07:59:56.3	–60:52:17.83	0.83 ± 0.13	8.86	104.87	13.08	
120	07:58:27.54	–60:52:19.13	0.53 ± 0.06	12.82	268.81	5.26	
121	07:58:13.86	–60:52:17.62	0.27 ± 0.05	9.49	263.72	5.11	
122	07:58:56.57	–60:52:15.49	0.98 ± 0.09	15.88	224.55	6.95	
123	07:57:18.27	–60:52:12.83	0.32 ± 0.06	7	147.54	8.78	U
124	07:57:29.35	–60:52:11.64	4.52 ± 0.21	41.44	145.8	7.7	U
125	07:58:16.66	–60:52:12.11	0.3 ± 0.05	10.32	272.54	5	
126	07:58:0.31	–60:52:12.04	2.67 ± 0.12	44.93	253.55	5.42	
127	07:59:15.24	–60:52:5.23	0.37 ± 0.06	10.64	201.76	8.57	
128	07:57:38.65	–60:52:3.25	0.36 ± 0.06	7.56	170.89	6.77	

Table A.1. continued.

Num	RA J2000	Dec J2000	Count rate cts ks^{-1}	Signif.	Exp. time ks	Offaxis arcmin	Un.
129	07:59:6.91	–60:52:1.81	0.85 ± 0.08	17.61	201.75	7.73	
130	07:59:59.25	–60:51:59.47	0.17 ± 0.05	5.21	105.55	13.3	U
131	07:58:19.33	–60:52:0.08	0.47 ± 0.06	10.55	261.88	4.81	
132	07:58:10.58	–60:51:57.53	2.68 ± 0.11	43.78	268.69	4.83	
133	07:59:17.95	–60:51:49.28	0.12 ± 0.03	6	195.26	8.7	U
135	07:57:2.9	–60:51:43.16	0.42 ± 0.08	7.16	161.57	10.14	
136	08:00:23.66	–60:51:40.36	1.38 ± 0.32	5.69	35.34	16.02	U
137	07:56:22.68	–60:51:38.88	4.4 ± 0.63	12.03	20.12	14.67	
138	07:56:41.56	–60:51:37.91	1.13 ± 0.17	9.43	66.07	12.49	
139	07:57:47.22	–60:51:38.92	0.39 ± 0.06	9.2	242.91	5.77	
140	07:58:33.36	–60:51:31	0.7 ± 0.07	15.44	218.55	4.73	
141	07:58:22.33	–60:51:27.9	4.03 ± 0.15	54.38	225.94	4.3	
142	07:57:28.31	–60:51:24.19	2.06 ± 0.13	25.52	213.02	7.31	
143	07:56:47.85	–60:51:9.76	0.61 ± 0.11	7.48	114.54	11.61	
144	07:57:39.91	–60:51:5.08	0.44 ± 0.08	6.62	236.46	6	
145	07:57:25.43	–60:51:1.44	0.24 ± 0.05	6.83	204.78	7.4	
146	07:59:9.6	–60:50:53.48	1.08 ± 0.09	20.55	196.28	7.35	
147	07:57:49.23	–60:50:53.81	0.56 ± 0.08	9.33	222.08	5.05	
148	07:59:20.99	–60:50:53.02	2.05 ± 0.13	24.98	195.36	8.58	
149	07:57:10.62	–60:50:52.58	0.57 ± 0.09	7.67	180.66	8.93	
150	07:58:41.79	–60:50:47.98	1.09 ± 0.08	17.9	265.38	4.67	
151	07:57:33.56	–60:50:42.47	0.34 ± 0.07	7.16	210.8	6.39	
153	08:00:4.18	–60:50:31.45	2.36 ± 0.22	16.5	84.17	13.43	
154	07:57:56.73	–60:50:33.94	1.85 ± 0.11	28.81	191.4	4.2	
155	07:59:42.51	–60:50:28.5	0.4 ± 0.08	6.34	150.04	10.88	
156	07:58:15.51	–60:50:29.44	0.13 ± 0.03	6.64	290.43	3.3	
157	07:57:36.04	–60:50:26.41	0.68 ± 0.08	12.14	220.81	5.99	
158	07:58:48.38	–60:50:25.91	0.57 ± 0.06	13.39	263.85	4.97	
159	07:58:36.48	–60:50:19.25	3.02 ± 0.12	51.5	274.35	3.89	
161	07:58:8.08	–60:50:14.06	0.09 ± 0.02	6.33	287.9	3.24	
162	07:56:30.54	–60:50:10.86	2.03 ± 0.25	10.96	55.51	13.37	
163	07:57:29.61	–60:50:11.58	1.88 ± 0.11	30.41	218.49	6.55	
164	07:56:53.39	–60:50:8.09	0.76 ± 0.12	8.18	138.31	10.66	
165	07:58:17.62	–60:50:5.96	0.35 ± 0.05	9.65	293.55	2.9	
166	07:58:11.54	–60:50:1.43	0.68 ± 0.07	17.21	292.01	2.91	
167	07:56:59.36	–60:49:55.96	1.84 ± 0.13	22.94	157.8	9.9	
168	07:58:41.79	–60:49:57.18	0.33 ± 0.05	8.33	279.63	4.05	
169	07:59:8.18	–60:49:55.49	0.19 ± 0.04	7.23	229.12	6.76	
170	07:57:43.53	–60:49:46.2	0.91 ± 0.07	19.44	255.78	4.87	
171	07:57:23.26	–60:49:39.07	1.8 ± 0.11	27.66	207.43	7.04	
172	07:57:57.93	–60:49:37.02	0.23 ± 0.04	7.18	251.49	3.39	
173	07:59:35.43	–60:49:30.94	0.32 ± 0.07	5.27	173.18	9.79	U
174	07:58:10.64	–60:49:32.3	0.46 ± 0.05	13.22	295.17	2.48	
175	07:59:56.69	–60:49:29.75	1.04 ± 0.13	12.49	119.94	12.32	
176	07:58:50.57	–60:49:28.67	13.91 ± 0.25	130.17	267.21	4.64	
177	07:59:2.1	–60:49:27.98	0.92 ± 0.09	14.57	219.85	5.9	
178	07:58:33.49	–60:49:25.57	0.23 ± 0.04	9.28	240.52	2.96	
180	07:59:47.66	–60:49:23.16	0.5 ± 0.08	8.54	124.79	11.22	
181	07:58:54.42	–60:49:14.45	0.11 ± 0.03	5.35	264.28	4.95	U
182	07:57:34.18	–60:49:10.34	0.6 ± 0.07	12.74	238.48	5.63	
183	07:57:10.91	–60:49:9.37	0.79 ± 0.09	13.41	179.36	8.34	
184	07:59:35.67	–60:49:8.62	0.45 ± 0.07	10.92	174.61	9.74	
185	07:58:29.74	–60:49:1.7	3.13 ± 0.12	54.33	296.25	2.37	
186	07:56:46.22	–60:48:58.39	4.29 ± 0.22	33.1	136.46	11.26	
187	07:59:17.96	–60:48:58.93	0.22 ± 0.05	5.87	213.48	7.6	
188	07:59:21.29	–60:48:57.06	5.66 ± 0.19	59.3	201.57	7.98	
189	07:56:38.58	–60:48:52.02	1.58 ± 0.16	14.34	94.92	12.17	
190	07:58:32.82	–60:48:53.03	0.41 ± 0.05	15.03	240.56	2.52	
191	07:59:32.03	–60:48:46.87	8.85 ± 0.27	75.1	162.35	9.24	

Table A.1. continued.

Num	RA J2000	Dec J2000	Count rate cts ks^{-1}	Signif.	Exp. time ks	Offaxis arcmin	Un.
192	07:58:2.67	–60:48:47.34	1.18 ± 0.08	25.64	290.03	2.4	
193	07:57:19.72	–60:48:46.55	2.31 ± 0.13	32.55	186.44	7.21	
194	07:57:46.28	–60:48:42.23	0.56 ± 0.07	10.21	264.75	4.08	
195	07:58:51.09	–60:48:38.16	0.23 ± 0.04	8.21	262.96	4.35	U
196	07:58:4.95	–60:48:33.41	0.25 ± 0.04	10.91	294.87	2.04	
197	07:57:30.96	–60:48:32.62	3.26 ± 0.15	43.51	204.17	5.82	
198	07:58:23.18	–60:48:28.12	0.24 ± 0.04	7.31	302.07	1.45	
199	07:57:55.48	–60:48:27.32	4.34 ± 0.15	59.22	239.54	2.95	
200	07:58:6.82	–60:48:24.73	1.69 ± 0.1	28.6	296.27	1.77	
201	07:58:38.9	–60:48:23.83	0.23 ± 0.04	9.04	214.92	2.88	
202	07:57:18.65	–60:48:15.16	1.66 ± 0.12	24.46	177.07	7.25	
203	07:57:36.17	–60:48:13.5	0.6 ± 0.07	13.25	238.72	5.13	
204	07:56:51.64	–60:48:11.27	0.54 ± 0.1	6.35	150.16	10.51	
205	07:58:36.72	–60:48:6.8	0.84 ± 0.08	15.91	289.11	2.52	
206	07:56:34.62	–60:48:3.89	11.17 ± 0.45	53.27	78.7	12.57	
207	07:57:9.5	–60:48:3.49	0.83 ± 0.09	13.6	184.72	8.33	
208	07:59:9.2	–60:47:57.52	0.44 ± 0.07	9.23	190.87	6.36	
209	07:59:27.66	–60:47:49.2	1.97 ± 0.13	26.07	173.32	8.59	
210	07:59:2.85	–60:47:49.63	0.49 ± 0.06	11.4	244.1	5.58	
211	07:58:48.85	–60:47:48.08	0.62 ± 0.06	15.41	279.05	3.88	
212	07:56:34.51	–60:47:39.66	3.8 ± 0.29	26.97	80.44	12.56	
213	07:58:5.31	–60:47:41.03	0.41 ± 0.05	10.93	297.17	1.55	
214	07:59:15.89	–60:47:35.41	0.6 ± 0.08	12.67	200.48	7.14	
215	07:59:49.84	–60:47:33.9	1.27 ± 0.12	17.7	148.98	11.28	U
216	07:59:23.26	–60:47:32.86	2.55 ± 0.13	34.32	203.47	8.04	
217	07:57:44.11	–60:47:28.28	2.95 ± 0.12	47.12	254.42	4.07	
218	07:59:36.62	–60:47:24.29	0.18 ± 0.04	6.19	170.23	9.67	
219	07:58:31.08	–60:47:24.9	0.35 ± 0.05	11.46	247.23	1.68	
220	07:58:56.49	–60:47:24	0.83 ± 0.07	17.92	252.5	4.77	
221	07:59:1.41	–60:47:22.31	0.27 ± 0.05	8.91	215.13	5.37	
222	07:57:30.89	–60:47:19.9	0.3 ± 0.05	8.45	222.91	5.68	
223	07:56:54.49	–60:47:18.71	1.06 ± 0.13	12.79	137.9	10.12	
224	07:57:37.23	–60:47:16.94	0.24 ± 0.05	6.77	225.45	4.9	
225	07:57:15.94	–60:47:12.01	0.97 ± 0.11	12.46	180.17	7.5	
226	07:59:5.97	–60:47:7.73	1.2 ± 0.09	24.14	231.67	5.92	U
227	07:56:38.93	–60:47:5.82	0.41 ± 0.1	5.55	80.03	12.02	
228	07:56:59.56	–60:47:0.53	1.96 ± 0.14	20.01	164.93	9.5	
229	07:57:52.55	–60:46:58.04	0.21 ± 0.05	5.95	258.69	3.04	
230	07:58:35.76	–60:46:53.65	4.02 ± 0.14	56.6	261.89	2.26	
231	07:58:16.89	–60:46:51.64	0.89 ± 0.07	21.27	268.79	0.35	
232	07:58:8.28	–60:46:49.69	0.58 ± 0.06	14.45	293.98	1.18	
233	07:58:23.58	–60:46:49.51	0.32 ± 0.05	9.28	291.63	0.84	
234	07:59:21.63	–60:46:47.32	0.75 ± 0.08	13.09	202.89	7.85	
235	07:57:25.14	–60:46:47.6	1.06 ± 0.1	14.65	192.35	6.39	
236	07:58:2.45	–60:46:47.39	5.04 ± 0.15	73.96	281.77	1.87	
237	07:58:5.48	–60:46:47.32	0.17 ± 0.04	8.67	295.31	1.51	U
238	07:58:31.75	–60:46:45.98	0.17 ± 0.03	7.95	271.03	1.8	
239	07:57:30.97	–60:46:45.52	0.33 ± 0.06	7.52	209.12	5.69	
240	07:57:20.82	–60:46:44.87	0.33 ± 0.05	8.63	206.71	6.92	
241	07:56:38.81	–60:46:39.9	1.03 ± 0.14	11.26	93.3	12.05	
242	07:57:39.73	–60:46:39.61	1.1 ± 0.08	22.62	246.88	4.63	
243	07:58:44.02	–60:46:37.16	0.22 ± 0.04	8.04	277.44	3.3	
244	07:58:20.26	–60:46:34.61	0.18 ± 0.04	6.46	307.78	0.71	
245	07:56:47.83	–60:46:31.8	4.07 ± 0.22	31.99	135.29	10.95	
246	07:58:36.95	–60:46:27.62	0.46 ± 0.06	13.85	281.05	2.5	
247	07:58:33.38	–60:46:25.93	0.7 ± 0.06	18.85	283.26	2.09	
248	08:00:3.87	–60:46:21.97	3.22 ± 0.24	20.38	88.02	13.02	
249	07:58:20.67	–60:46:21.86	0.41 ± 0.06	9.09	285.1	0.93	
250	08:00:16.2	–60:46:17	1.84 ± 0.25	9.81	61.28	14.53	

Table A.1. continued.

Num	RA J2000	Dec J2000	Count rate cts ks^{-1}	Signif.	Exp. time ks	Offaxis arcmin	Un.
251	07:59:6.29	–60:46:17.36	0.4 ± 0.06	9.19	214.8	6.03	
252	07:58:5.06	–60:46:12.29	1.79 ± 0.1	33.08	261.96	1.81	
254	07:57:53.4	–60:46:9.91	1.4 ± 0.1	23.97	243.57	3.11	
255	07:57:29.22	–60:46:7.14	0.63 ± 0.08	13.96	208.75	5.98	
256	07:59:22.99	–60:46:6.56	0.16 ± 0.04	6.79	193	8.08	
257	07:59:21.69	–60:46:5.09	1.99 ± 0.14	23.38	185.71	7.92	
258	07:56:34.22	–60:45:59.9	1.27 ± 0.19	9.7	76.86	12.65	
259	07:58:32.3	–60:46:1.52	3.8 ± 0.14	50.59	263.77	2.16	
260	07:57:58.33	–60:45:45.22	0.74 ± 0.07	18.58	255.16	2.74	
261	07:57:42.98	–60:45:40.72	1.51 ± 0.1	28.93	244.51	4.47	
262	07:57:26.11	–60:45:39.42	1.03 ± 0.1	15.23	185.82	6.45	
263	07:58:44.07	–60:45:38.23	0.77 ± 0.07	17.36	250.56	3.61	
264	07:59:38.96	–60:45:36.32	0.24 ± 0.06	5.28	159.08	10.08	
265	07:57:49.69	–60:45:36.18	0.56 ± 0.06	12.6	251.36	3.74	U
266	07:59:53.23	–60:45:32.04	0.57 ± 0.12	5.59	125.82	11.81	
267	07:59:40.91	–60:45:28.51	1.67 ± 0.14	17.76	156.12	10.34	U
268	07:57:2.64	–60:45:28.01	1.42 ± 0.12	19.12	166.65	9.29	
269	07:59:22.38	–60:45:27.32	2.1 ± 0.13	28.73	184.81	8.12	
270	07:58:13.99	–60:45:24.66	0.34 ± 0.04	11.56	295.02	1.84	
271	07:58:39.02	–60:45:21.89	0.28 ± 0.05	8.13	286.39	3.21	
272	08:00:4.9	–60:45:19.22	2.18 ± 0.23	14	76.49	13.25	
273	07:59:17.69	–60:45:20.27	1.02 ± 0.09	17.71	211.1	7.59	
274	08:00:14.59	–60:45:17.03	2.73 ± 0.28	14.4	63.91	14.43	
275	07:58:18.18	–60:45:15.98	3.71 ± 0.13	59.99	283.31	1.94	
276	07:58:26.98	–60:45:10.87	0.6 ± 0.06	13.95	260.92	2.33	
277	07:57:56.21	–60:45:9.65	0.08 ± 0.02	5.07	274.52	3.3	
278	07:57:43.49	–60:45:8.5	0.25 ± 0.05	6.28	242.89	4.63	
279	07:57:54.75	–60:45:8.39	1.02 ± 0.08	16.37	264.79	3.45	
280	07:56:33.6	–60:45:3.38	1.46 ± 0.19	11.51	64.62	12.85	
282	07:57:12.86	–60:45:3.38	0.93 ± 0.11	13.84	176.37	8.17	
283	07:58:4.96	–60:45:2.41	0.65 ± 0.06	14.24	282.14	2.64	
284	07:57:25.4	–60:45:0.5	4.37 ± 0.18	45.79	202.66	6.72	
285	07:59:47.73	–60:44:54.38	1.32 ± 0.14	12.96	139.12	11.26	
286	07:56:58.47	–60:44:54.64	0.31 ± 0.07	6.23	152.95	9.91	
287	07:59:10.92	–60:44:47.22	0.93 ± 0.09	16.74	199.44	6.96	
289	07:58:33.66	–60:44:42.18	0.21 ± 0.04	9.54	287.46	3.19	
290	07:58:8.84	–60:44:40.06	3.35 ± 0.13	46.74	265.18	2.74	
291	07:58:17.41	–60:44:38.18	0.29 ± 0.05	5.79	252.64	2.57	
292	07:59:36.59	–60:44:33.5	8.91 ± 0.28	61.96	159.45	10.02	
293	07:59:59.39	–60:44:29.26	0.29 ± 0.07	6.7	100.61	12.74	
294	07:58:27.97	–60:44:31.24	0.31 ± 0.05	8.87	253.93	2.97	
295	07:58:33.53	–60:44:30.52	4.94 ± 0.15	62.45	285.06	3.33	
296	07:59:5.14	–60:44:27.56	0.81 ± 0.08	16.71	202.68	6.44	
297	07:58:21.14	–60:44:25.3	0.23 ± 0.04	8.24	282.62	2.82	
298	07:57:42.83	–60:44:20.65	1.25 ± 0.09	23.98	243.53	5.1	
299	07:57:39.33	–60:44:15.76	0.19 ± 0.04	8.04	209.34	5.5	U
300	07:57:57.41	–60:44:15.68	2.24 ± 0.11	39.23	267.02	3.82	
301	07:58:50.43	–60:44:14.57	0.21 ± 0.05	5.4	257.22	5	U
302	07:58:26.01	–60:44:13.24	0.2 ± 0.04	8.67	287.2	3.16	
303	07:57:9.98	–60:44:11.58	1.23 ± 0.12	15.09	171.23	8.77	
304	07:59:0.72	–60:44:11.76	0.37 ± 0.06	8.41	222.52	6.08	
305	07:57:20.82	–60:44:3.8	1.95 ± 0.12	28.13	190.75	7.59	
306	07:58:22.61	–60:44:4.13	0.59 ± 0.07	13.78	278.19	3.2	
307	07:57:1.08	–60:43:46.85	1.02 ± 0.11	14.09	154.8	9.93	U
308	07:59:2.9	–60:43:46.27	0.38 ± 0.05	11.1	230.18	6.53	
309	07:57:5.71	–60:43:40.94	0.44 ± 0.08	6.74	144.62	9.44	
310	07:59:50.05	–60:43:35.69	0.2 ± 0.07	5.01	134.29	11.87	
311	07:58:14.63	–60:43:33.1	0.94 ± 0.08	19.78	241.54	3.67	
312	07:59:2.15	–60:43:25.64	0.28 ± 0.05	8.11	223.79	6.64	

Table A.1. continued.

Num	RA J2000	Dec J2000	Count rate cts ks^{-1}	Signif.	Exp. time ks	Offaxis arcmin	Un.
313	07:56:47.14	–60:43:22.4	1.86 ± 0.17	18.96	95.02	11.67	
314	07:59:51.66	–60:43:21.65	13.23 ± 0.39	71.49	126.17	12.13	
315	07:57:36.11	–60:43:21.72	0.29 ± 0.06	5.97	200.01	6.34	
316	07:57:52.61	–60:43:19.49	1.46 ± 0.11	20.74	221.21	4.92	
317	07:58:39.77	–60:43:16.68	0.85 ± 0.08	15.73	262.49	4.78	
318	07:59:34.35	–60:43:11.78	0.37 ± 0.07	6.28	162.52	10.21	U
319	07:58:22.15	–60:43:12.07	0.27 ± 0.05	7.53	272.96	4.04	
320	07:59:39.19	–60:43:8.04	0.25 ± 0.06	5.08	155.1	10.78	
321	07:58:41.69	–60:43:9.37	0.17 ± 0.04	6.01	258.73	5.01	
322	07:57:45.54	–60:43:8.33	0.51 ± 0.07	10.62	214.93	5.63	
323	07:58:57.58	–60:42:59.69	7.58 ± 0.21	80.27	225.83	6.46	
324	07:58:1.65	–60:42:53.03	0.94 ± 0.08	16.34	251.95	4.73	
325	07:58:53.63	–60:42:51.3	0.19 ± 0.04	5.86	237.45	6.2	
326	07:57:53.85	–60:42:48.82	0.66 ± 0.07	17.37	243.92	5.25	U
327	08:00:20.75	–60:42:36.4	3.02 ± 0.5	10.27	19.42	15.75	
328	07:59:29.87	–60:42:37.01	0.61 ± 0.09	10.39	168.59	9.97	
329	07:57:47.25	–60:42:37.98	1.87 ± 0.11	25.24	231.32	5.87	
330	07:58:39.93	–60:42:35.14	0.89 ± 0.08	18.36	253.09	5.37	U
331	07:59:40.11	–60:42:31.25	2.63 ± 0.18	28.12	127.62	11.13	
332	07:57:56.18	–60:42:31.93	1.7 ± 0.11	22.98	242.74	5.34	
333	07:57:12.79	–60:42:23.76	0.56 ± 0.1	6.61	146.37	9.24	
334	07:59:11.83	–60:42:22.46	4.04 ± 0.17	48.75	189.77	8.21	
336	07:58:49.57	–60:42:13.9	2.1 ± 0.12	30.92	209.03	6.34	
337	07:57:51.3	–60:42:12.67	0.49 ± 0.07	10.31	229.8	5.92	
338	07:57:26.74	–60:42:11.48	0.62 ± 0.09	8.78	188.27	7.96	
339	07:57:31.38	–60:42:10.66	0.25 ± 0.05	7.01	198.54	7.54	
340	07:58:53.98	–60:42:8.14	0.67 ± 0.07	13.58	217.1	6.75	
341	07:58:34.83	–60:42:6.12	0.34 ± 0.05	9.98	247.87	5.53	
342	07:59:55.79	–60:41:59.39	2.97 ± 0.22	22.13	112.97	13.1	
343	07:58:19.97	–60:41:58.16	3.42 ± 0.14	49.59	225.66	5.24	
344	07:57:49.01	–60:41:55.64	0.62 ± 0.07	13.79	195.48	6.31	
346	07:58:30.25	–60:41:50.5	3.79 ± 0.15	51.78	228.89	5.58	
347	07:58:40.45	–60:41:45.96	1.97 ± 0.12	26.95	239.31	6.12	
348	07:58:43.28	–60:41:45.6	0.65 ± 0.08	12.93	235.91	6.29	
349	07:58:45.64	–60:41:41.53	0.21 ± 0.04	8.66	233.29	6.5	
350	07:58:20.36	–60:41:39.05	0.31 ± 0.06	9.37	233.35	5.56	
351	07:59:5.8	–60:41:26.52	0.26 ± 0.06	5.68	198.54	8.25	
352	07:56:24.15	–60:41:21.23	3.73 ± 0.71	10.89	12.46	15.03	
353	07:59:15.66	–60:41:20.76	0.83 ± 0.11	10.77	174.03	9.22	
354	07:59:23.84	–60:41:18.92	0.9 ± 0.11	11	164.45	10.03	
355	07:59:53.05	–60:41:17.63	0.8 ± 0.14	7.17	115.23	13.09	
356	07:58:3.78	–60:41:13.52	0.46 ± 0.07	9.12	202.41	6.2	U
357	07:57:32.66	–60:41:11.8	2.16 ± 0.14	22.4	169.59	8.12	U
358	07:57:47.65	–60:41:11.62	0.73 ± 0.09	10.47	197.55	7.02	
360	07:58:57.73	–60:41:0.13	0.56 ± 0.07	11.26	204.22	7.92	
361	08:00:1.87	–60:40:57.58	0.2 ± 0.06	5.22	82.92	14.21	
362	07:57:9.28	–60:40:54.26	0.49 ± 0.09	7.44	135.48	10.44	
363	07:57:14.22	–60:40:53	4.18 ± 0.2	43.14	147.67	9.98	
364	07:57:18.48	–60:40:52.68	0.5 ± 0.07	10.01	155.73	9.58	
365	07:59:40.6	–60:40:47.5	0.32 ± 0.09	5.28	112.57	12.02	U
366	07:58:0.54	–60:40:44.11	1.38 ± 0.11	25.18	179.85	6.79	U
367	07:57:55.72	–60:40:39.79	1.31 ± 0.1	22.68	214.6	7.06	
368	08:00:5.07	–60:40:31.44	1.17 ± 0.22	6.88	53.08	14.75	
369	07:59:31.05	–60:40:27.16	0.17 ± 0.05	5.62	119.16	11.25	
370	07:59:13.56	–60:40:25.07	0.47 ± 0.07	10.21	157.02	9.65	
371	07:58:42.66	–60:40:22.12	0.53 ± 0.09	7.16	178.93	7.5	
372	07:58:23.02	–60:40:21	5.8 ± 0.19	63.43	215.54	6.89	
373	07:58:2.58	–60:40:14.48	0.94 ± 0.09	15.37	210.84	7.19	
374	07:58:33.48	–60:40:13.48	0.35 ± 0.06	7.29	192.3	7.25	U

Table A.1. continued.

Num	RA J2000	Dec J2000	Count rate cts ks^{-1}	Signif.	Exp. time ks	Offaxis arcmin	Un.
375	08:00:0	–60:40:9.66	0.92 ± 0.19	6.95	49.79	14.38	
376	07:58:8.15	–60:40:9.8	0.2 ± 0.05	6.16	198.9	7.13	
377	07:58:17.16	–60:40:6.56	0.3 ± 0.07	6.32	185.92	7.09	
378	07:56:59.13	–60:39:58.61	0.39 ± 0.1	5	94.95	11.99	
379	07:57:47.75	–60:39:59.83	0.34 ± 0.07	7.11	124.98	8.07	
380	07:56:55.67	–60:39:52.67	0.16 ± 0.05	5.04	92.59	12.39	
381	07:57:24.36	–60:39:51.48	1.15 ± 0.12	16.21	154.19	9.8	
383	07:57:25.96	–60:39:48.35	2.46 ± 0.16	24.83	157.79	9.71	
384	07:59:28.97	–60:39:40.57	1.28 ± 0.14	12.99	121.71	11.54	
385	07:57:10.76	–60:39:36.14	1.03 ± 0.13	13.33	107.16	11.14	
386	07:58:20.69	–60:39:36.25	0.61 ± 0.08	10.9	175.56	7.61	U
387	07:56:55.51	–60:39:34.2	0.71 ± 0.14	6.88	90.61	12.59	
388	07:58:42.72	–60:39:33.88	0.5 ± 0.07	10.52	192.15	8.24	
389	07:58:52.46	–60:39:33.26	0.49 ± 0.08	8.15	154.02	8.77	
390	07:58:37.74	–60:39:22.25	0.42 ± 0.08	6.88	164.73	8.22	
391	07:57:28.74	–60:39:10.94	0.37 ± 0.08	6.04	139.96	9.99	
392	07:57:46.16	–60:39:8.5	0.26 ± 0.06	6.04	157.08	8.92	U
393	07:56:38.94	–60:39:4.07	1.18 ± 0.23	7.65	39.83	14.53	
394	07:59:7.75	–60:39:4.25	0.89 ± 0.1	14.01	153.66	10.2	
395	07:58:46.21	–60:39:2.52	0.22 ± 0.05	5.09	188.34	8.89	
396	07:57:15.77	–60:38:53.34	1.99 ± 0.18	17.3	107.24	11.22	
397	07:58:36.21	–60:38:46.1	1.1 ± 0.1	16.44	180.67	8.74	
398	07:58:12.53	–60:38:38.18	1.69 ± 0.13	18.66	185.12	8.59	
399	07:58:50.49	–60:38:37.9	17.99 ± 0.37	105.34	169.12	9.48	
400	07:57:40.72	–60:38:31.27	0.51 ± 0.1	6.72	104.33	9.77	
401	07:59:7.72	–60:38:30.12	0.29 ± 0.06	5.82	132.1	10.65	
402	07:57:30.98	–60:38:26.45	1.38 ± 0.15	14.48	110.62	10.44	
403	07:58:4.35	–60:38:26.88	0.83 ± 0.1	11.28	132.88	8.9	
404	07:59:22.15	–60:38:23.32	0.44 ± 0.09	6.79	128.88	11.85	
405	07:58:34.06	–60:38:17.27	0.55 ± 0.08	9.16	165.47	9.14	
406	07:57:20.04	–60:38:11.11	0.63 ± 0.12	7.19	104.47	11.43	
407	07:57:52.14	–60:38:8.38	0.41 ± 0.09	6.11	133.56	9.57	
408	07:58:13.05	–60:38:6.61	0.21 ± 0.05	6.12	145.54	9.11	
409	07:58:31.01	–60:37:46.74	1.76 ± 0.14	24.95	135.62	9.57	
410	07:59:49.56	–60:37:44.54	2.53 ± 0.25	15.35	67.61	14.71	U
411	07:56:58.15	–60:37:45.01	0.74 ± 0.15	7.25	60.81	13.54	
412	07:59:55.85	–60:37:43.82	0.53 ± 0.14	5.36	44.16	15.32	
413	07:57:32.27	–60:37:21.36	0.87 ± 0.11	14.03	105.73	11.29	
414	07:58:23.55	–60:37:20.06	2.99 ± 0.17	34.31	128.72	9.9	
415	07:58:19.39	–60:37:18.16	0.31 ± 0.08	5.68	118.93	9.9	
416	07:58:48.65	–60:37:15.02	0.53 ± 0.1	6.41	127.15	10.66	
417	07:58:32.1	–60:37:14.77	0.4 ± 0.08	6.76	133.63	10.12	
418	07:59:22.41	–60:37:10.81	0.59 ± 0.11	7.34	91.59	12.79	
419	07:59:4.76	–60:37:8.54	0.58 ± 0.1	8.26	115.3	11.61	
420	07:56:36.65	–60:36:47.84	6.79 ± 0.8	17.26	21.09	16.13	
422	07:57:50.23	–60:36:34.81	0.17 ± 0.05	5.96	113.36	11.13	
423	07:57:47.84	–60:36:34.52	2.48 ± 0.19	21.57	112.29	11.23	
425	07:58:57.63	–60:36:13.36	2.56 ± 0.19	23.82	111.21	12.03	
426	07:58:53.28	–60:36:11.2	3.47 ± 0.22	30.42	110.78	11.86	
427	07:57:29.36	–60:36:3.02	1.18 ± 0.15	12.82	80.36	12.61	
428	07:57:55.14	–60:36:0.11	2.02 ± 0.17	17.81	108.16	11.53	
429	07:58:14.54	–60:35:58.42	2 ± 0.16	22.19	117.31	11.23	U
430	07:58:6.3	–60:35:53.16	13.57 ± 0.4	80.24	113.98	11.4	
431	07:58:24.01	–60:35:48.37	1.2 ± 0.16	10.91	91.3	11.42	
432	07:58:18.2	–60:35:38.08	0.41 ± 0.09	6.16	110.51	11.57	
433	07:58:11.5	–60:35:31.99	0.37 ± 0.08	6.97	111.82	11.69	
434	07:58:51.97	–60:35:20.69	5.97 ± 0.29	37.16	105.24	12.59	
435	07:58:41.92	–60:35:16.8	0.61 ± 0.12	6.31	99.38	12.29	U
436	07:58:16.44	–60:35:6.54	0.3 ± 0.07	5.59	107.99	12.09	

Table A.1. continued.

Num	RA J2000	Dec J2000	Count rate cts ks^{-1}	Signif.	Exp. time ks	Offaxis arcmin	Un.
437	07:58:4.74	–60:35:4.81	0.84 ± 0.12	10.19	105.08	12.22	
439	07:59:19.8	–60:34:43.82	12.96 ± 0.51	50.19	73.5	14.62	
440	07:57:24.66	–60:34:33.89	0.46 ± 0.12	6.28	65.16	14.19	
441	07:57:47.03	–60:34:33.92	1.01 ± 0.14	10.62	76.28	13.17	
442	07:59:24.3	–60:34:32.34	0.5 ± 0.11	7.36	61.2	15.08	
444	07:58:14.87	–60:34:19.42	0.5 ± 0.11	6.22	97.79	12.88	U
445	07:57:23.92	–60:34:17.83	1.55 ± 0.24	9.41	54.3	14.47	
446	07:58:32.21	–60:34:11.96	0.48 ± 0.11	7.13	96.96	13.13	
447	07:57:31.02	–60:34:8.76	1.28 ± 0.21	7.74	45.3	14.24	
448	07:58:10.21	–60:34:0.34	0.54 ± 0.09	8.39	95.92	13.23	
449	07:58:55.73	–60:33:45.83	1.27 ± 0.19	11.93	61.5	14.23	
450	07:58:2.77	–60:33:43.49	2.08 ± 0.2	16.56	90.51	13.6	U
451	07:58:50.88	–60:33:31.03	0.89 ± 0.14	8.99	72.22	14.28	
453	07:57:12.74	–60:33:6.7	4.32 ± 0.62	16.55	21.34	16.16	
455	07:59:8.82	–60:33:1.22	0.72 ± 0.16	6.73	58.63	15.52	
456	07:58:43.69	–60:32:56.4	4.13 ± 0.3	26.79	67.19	14.62	
459	07:58:36.65	–60:32:20.76	0.79 ± 0.17	5.66	66.53	15.04	U
460	07:58:42.41	–60:32:18.96	0.96 ± 0.16	8.46	65.62	15.2	
461	07:59:11.91	–60:31:38.96	2.26 ± 0.53	7.71	16.16	16.92	
462	07:57:47.61	–60:31:33.89	3.93 ± 0.66	10.79	16.38	16.06	
464	07:57:36.22	–60:30:16.38	3.34 ± 0.65	8.64	14.93	17.67	U

Appendix B: Identifications, X-ray fluxes and luminosities of NGC 2516 stars

Table B.1. Identifications, X-ray fluxes and luminosities of NGC 2516 X-ray detected stars. Columns report: X source identifier (as in Table A.1, identifier from Jeffries et al. 2001), match distance, V, $B-V$, $V-I$, fluxes, luminosities in the 0.3–7.9 keV band, log $L_{\rm bol}$ and the ratio log $L_{\rm X}/L_{\rm bol}$. Errors are propagated from count rates, for systematic errors see discussion in Sect. 2.2. Exposure times are calculated from the summed exposures, scaling pn to MOS with a factor of 3.6 as described in the text.

X-ray Src	Opt. Id.	Distance arcsec	V mag	$B-V$ mag	$V-I$ mag	$f_{\rm X}$ (0.3–7.9 keV) 10^{-15} erg s^{-1} cm^{-2}	log $L_{\rm X}$ erg s^{-1}	log $L_{\rm bol}$ erg s^{-1}	log $L_{\rm X}/L_{\rm bol}$
6	6160	1	20.9	...	3.06	67 ± 7	$30.08^{0.04}_{-0.05}$	31.52	–1.44
7	7036	3.8	13	0.7	0.81	6 ± 2	$29.02^{0.1}_{-0.1}$	33.9	–4.88
8	9114	5.9	13.1	0.7	0.8	18 ± 3	$29.52^{0.06}_{-0.07}$	33.93	–4.41
10	8793	2.3	20.1	...	3.02	11 ± 2	$29.29^{0.07}_{-0.08}$	31.54	–2.24
11	9544	3.5	17.5	1.5	2.25	6.5 ± 2	$29.07^{0.1}_{-0.2}$	31.94	–2.87
12	6976	4.3	12.8	0.6	0.78	46 ± 4	$29.91^{0.03}_{-0.04}$	33.97	–4.05
15	6871	5.4	14.8	1.2	1.34	7 ± 2	$29.1^{0.1}_{-0.1}$	32.93	–3.83
16	7682	1.3	19.4	...	2.64	10 ± 2	$29.25^{0.07}_{-0.09}$	31.68	–2.43
29	9015	3.7	16.8	1.5	1.76	10.1 ± 1	$29.26^{0.06}_{-0.07}$	32.55	–3.29
31	8126	2.6	15.6	1.2	1.36	3.7 ± 0.8	$28.82^{0.09}_{-0.1}$	32.91	–4.09
32	6689	2.1	10.9	0.3	-10	52 ± 4	$29.97^{0.03}_{-0.03}$	34.5	–4.53
38	8584	2	14.7	1.2	1.29	13.9 ± 1	$29.4^{0.04}_{-0.05}$	32.97	–3.58
39	11240	2.3	15	1	1.18	20.5 ± 3	$29.56^{0.05}_{-0.06}$	33.12	–3.55
41	8037	3.1	19.7	...	2.81	3.6 ± 0.8	$28.81^{0.08}_{-0.1}$	31.6	–2.79
43	8990	2.8	16.2	1.3	1.55	3.9 ± 0.8	$28.85^{0.08}_{-0.1}$	32.74	–3.89
46	5299	2.3	17.3	1.5	2.01	11.0 ± 2	$29.28^{0.07}_{-0.08}$	32.19	–2.91
59	10440	2.5	17.2	1.5	1.92	6.1 ± 1	$29.03^{0.07}_{-0.08}$	32.32	–3.29
60	7743	1	12.6	0.7	0.8	30.9 ± 1	$29.74^{0.02}_{-0.02}$	33.93	–4.18
61	6465	2.4	15.1	1.3	1.41	18 ± 2	$29.5^{0.04}_{-0.05}$	32.87	–3.37
63	5052	2.6	10.9	0.3	0.45	67 ± 5	$30.08^{0.03}_{-0.04}$	34.48	–4.4
65	9911	1.5	18.4	1.6	2.62	9.2 ± 1	$29.22^{0.04}_{-0.05}$	31.68	–2.47
68	7194	1.6	11.4	0.4	0.57	2.9 ± 0.7	$28.71^{0.09}_{-0.1}$	34.32	–5.61
69	7312	6.7	13.8	0.8	0.92	6.8 ± 1	$29.09^{0.06}_{-0.07}$	33.63	–4.54
74	6514	0.4	16.4	1.4	1.6	3.0 ± 0.7	$28.73^{0.09}_{-0.1}$	32.69	–3.95
77	6265	1	17.3	1.5	2.02	13.2 ± 1	$29.38^{0.04}_{-0.04}$	32.18	–2.8
78	9696	1.2	12	0.5	0.59	5.8 ± 0.8	$29.02^{0.06}_{-0.06}$	34.3	–5.28
79	9465	0.2	13.8	0.8	0.96	98 ± 2	$30.24^{0.01}_{-0.01}$	33.5	–3.26
81	8462	4.1	20.7	...	3.23	2.9 ± 0.5	$28.71^{0.07}_{-0.08}$	31.46	–2.75
84	7619	0.8	14.3	0.9	1.01	12.6 ± 1	$29.35^{0.03}_{-0.04}$	33.38	–4.03
87	8411	0.9	14	0.9	0.94	2.7 ± 0.5	$28.68^{0.07}_{-0.09}$	33.56	–4.88
88	8689	6.6	13.9	1	1.05	2.1 ± 0.5	$28.57^{0.09}_{-0.1}$	33.32	–4.74
90	9908	1.6	16.9	1.5	2.09	14.1 ± 1	$29.4^{0.03}_{-0.03}$	32.1	–2.7
92	7548	0.6	20.3	...	3.18	1.7 ± 0.4	$28.48^{0.09}_{-0.1}$	31.48	–3.01
94	9676	1.9	14.3	0.9	1.05	57 ± 2	$30.01^{0.01}_{-0.01}$	33.31	–3.3
95	8479	1.1	19.2	...	2.62	2.5 ± 0.5	$28.65^{0.08}_{-0.1}$	31.69	–3.04
97	12201	3	19.6	...	2.95	12 ± 2	$29.34^{0.06}_{-0.07}$	31.56	–2.22
98	6426	2	19.8	...	2.75	2.0 ± 0.5	$28.56^{0.1}_{-0.1}$	31.61	–3.05
99	8991	1.8	10.5	0.2	0.25	11.6 ± 0.9	$29.32^{0.03}_{-0.03}$	34.73	–5.42
102	6322	3.4	13.2	0.9	0.94	5.4 ± 1	$28.99^{0.07}_{-0.09}$	33.56	–4.57
103	7678	1.6	14.4	0.9	1.05	31.3 ± 1	$29.75^{0.02}_{-0.02}$	33.31	–3.56
104	9852	1.1	12.1	0.7	0.76	24.7 ± 1	$29.65^{0.02}_{-0.02}$	34	–4.36
111	7932	2	18.8	1.6	2.44	6.2 ± 0.6	$29.05^{0.04}_{-0.05}$	31.79	–2.74
114	7051	0.8	20.2	...	3.26	7.4 ± 0.9	$29.12^{0.05}_{-0.05}$	31.45	–2.33
115	6628	1.7	19.1	...	2.75	2.0 ± 0.5	$28.55^{0.1}_{-0.1}$	31.62	–3.07
122	10017	0.5	17.4	1.6	2.16	9.4 ± 0.9	$29.22^{0.04}_{-0.04}$	32.01	–2.78
125	8404	0.8	18.9	...	2.51	2.8 ± 0.4	$28.7^{0.06}_{-0.07}$	31.74	–3.03
126	7782	0.2	15.8	1.4	1.71	58 ± 3	$30.01^{0.02}_{-0.02}$	32.6	–2.58
127	10688	0.8	10	0.1	0.16	3.5 ± 0.6	$28.79^{0.07}_{-0.08}$	34.92	–6.13
128	6970	2.6	19.8	...	2.94	3.4 ± 0.6	$28.78^{0.07}_{-0.08}$	31.56	–2.78
131	8502	0.7	15.2	1.1	1.23	4.5 ± 0.6	$28.9^{0.06}_{-0.06}$	33.05	–4.15
135	5576	1.4	19.5	...	2.98	4.0 ± 0.7	$28.86^{0.07}_{-0.09}$	31.55	–2.69
137	4125	3.3	11.6	0.5	0.66	42 ± 6	$29.87^{0.06}_{-0.07}$	34.15	–4.27
139	7276	1.1	16.4	1.4	1.63	3.7 ± 0.6	$28.82^{0.06}_{-0.07}$	32.66	–3.84
140	9035	3.2	18.6	...	2.63	6.7 ± 0.7	$29.08^{0.04}_{-0.05}$	31.68	–2.6
142	6570	5.3	13.4	0.7	0.87	19.6 ± 1	$29.55^{0.03}_{-0.03}$	33.77	–4.22

Table B.1. continued.

X-ray Src	Opt. Id.	Distance	V	$B-V$	$V-I$	f_X (0.3–7.9 keV)	log L_X	log L_{bol}	log L_X/L_{bol}
		arcsec	mag	mag	mag	10^{-15} erg s^{-1} cm^{-2}	erg s^{-1}	erg s^{-1}	
143	5066	3	18.4	1.6	2.38	5.8 ± 1	$29.02^{0.07}_{-0.08}$	31.85	–2.83
144	7006	1.4	20.2	...	3.03	4.1 ± 0.7	$28.87^{0.07}_{-0.09}$	31.53	–2.66
145	6473	2.3	19.4	1.6	2.72	2.3 ± 0.5	$28.62^{0.08}_{-0.1}$	31.63	–3.01
146	10471	1.9	17.5	1.4	2.08	10.2 ± 0.9	$29.26^{0.04}_{-0.04}$	32.11	–2.85
147	7358	3.3	17.8	1.5	2.13	5.3 ± 0.8	$28.98^{0.06}_{-0.07}$	32.06	–3.08
148	10857	0.7	19.3	...	2.88	19.5 ± 1	$29.54^{0.03}_{-0.03}$	31.58	–2.04
149	5901	2.8	13	0.7	0.8	5.5 ± 0.9	$28.99^{0.07}_{-0.08}$	33.93	–4.94
151	6751	2	18.7	1.6	2.44	3.2 ± 0.6	$28.76^{0.08}_{-0.1}$	31.79	–3.04
154	7650	0.6	12.7	0.6	0.77	22.1 ± 1	$29.6^{0.03}_{-0.03}$	33.99	–4.39
155	11556	1.5	16.2	1.4	1.55	3.8 ± 0.8	$28.83^{0.08}_{-0.1}$	32.74	–3.91
156	8370	2.2	20.8	...	3.16	1.2 ± 0.3	$28.34^{0.09}_{-0.1}$	31.49	–3.15
159	9175	0.9	11.7	0.6	0.7	38 ± 2	$29.84^{0.02}_{-0.02}$	34.09	–4.25
163	6605	2.3	13.6	0.8	0.96	17.8 ± 1	$29.5^{0.03}_{-0.03}$	33.51	–4.01
164	5261	5.5	15.1	1.1	1.22	7.3 ± 1	$29.11^{0.06}_{-0.07}$	33.08	–3.96
166	8192	2.8	13.9	0.9	0.95	6.5 ± 0.6	$29.06^{0.04}_{-0.04}$	33.54	–4.47
171	6373	1	11.3	0.5	0.66	17.1 ± 1	$29.49^{0.03}_{-0.03}$	34.15	–4.66
174	8172	0.4	12	0.5	0.68	4.4 ± 0.5	$28.9^{0.05}_{-0.05}$	34.1	–5.21
175	12005	1.6	11.6	0.6	0.62	9.9 ± 1	$29.25^{0.05}_{-0.06}$	34.24	–4.99
178	9048	1.6	10.8	0.3	0.36	2.2 ± 0.4	$28.6^{0.07}_{-0.09}$	34.58	–5.98
180	11713	1.9	12.4	0.7	0.8	4.7 ± 0.8	$28.93^{0.07}_{-0.08}$	33.93	–5
183	5899	2.6	18.4	1.5	2.37	7.5 ± 0.9	$29.13^{0.05}_{-0.05}$	31.85	–2.72
184	11348	0.6	19.2	...	2.61	4.3 ± 0.7	$28.89^{0.06}_{-0.07}$	31.69	–2.8
185	8893	1.2	16.2	1.4	1.82	37.5 ± 1	$29.83^{0.02}_{-0.02}$	32.47	–2.64
187	10753	1.5	13.7	0.8	0.9	2.1 ± 0.5	$28.58^{0.1}_{-0.1}$	33.71	–5.13
190	9025	0.6	17.5	1.6	1.97	3.9 ± 0.5	$28.84^{0.05}_{-0.06}$	32.22	–3.38
191	11233	1.9	13.9	0.8	1.02	80 ± 2	$30.16^{0.01}_{-0.01}$	33.36	–3.2
194	7231	3.2	11.2	0.4	0.49	5.3 ± 0.7	$28.98^{0.05}_{-0.06}$	34.44	–5.46
197	6649	0.9	14	0.8	0.98	41.6 ± 2	$29.87^{0.02}_{-0.02}$	33.45	–3.58
198	8647	1.7	20	...	3.11	2.2 ± 0.4	$28.6^{0.07}_{-0.09}$	31.51	–2.9
199	7585	0.8	12.9	0.7	0.88	46 ± 2	$29.91^{0.01}_{-0.02}$	33.76	–3.84
200	8036	1.8	17.6	...	2.41	16.1 ± 0.9	$29.46^{0.02}_{-0.03}$	31.81	–2.35
201	9283	0.6	16.9	1.4	1.84	2.2 ± 0.4	$28.59^{0.07}_{-0.08}$	32.45	–3.87
203	6852	1.2	13.7	0.8	0.91	5.7 ± 0.6	$29.01^{0.05}_{-0.05}$	33.68	–4.67
204	5179	1.1	19.6	...	2.78	5.2 ± 1	$28.97^{0.07}_{-0.09}$	31.61	–2.64
205	9185	1	18.3	1.5	2.27	8.0 ± 0.7	$29.16^{0.04}_{-0.04}$	31.93	–2.77
206	4598	0.5	14	0.9	1.02	120 ± 5	$30.33^{0.02}_{-0.02}$	33.37	–3.04
207	5833	1.2	12.4	0.6	0.72	7.9 ± 0.8	$29.15^{0.04}_{-0.05}$	34.06	–4.91
208	10452	1.2	19.7	...	2.97	4.1 ± 0.6	$28.87^{0.06}_{-0.07}$	31.55	–2.68
209	11082	2.6	9.6	0.1	0.08	18.7 ± 1	$29.53^{0.03}_{-0.03}$	35.3	–5.78
2-10	10210	1.3	10.8	0.3	0.33	4.7 ± 0.6	$28.92^{0.05}_{-0.06}$	34.62	–5.7
211	9703	1.4	18.5	1.6	2.48	5.9 ± 0.6	$29.02^{0.04}_{-0.04}$	31.75	–2.73
213	7962	1	12	0.5	0.65	3.9 ± 0.5	$28.85^{0.05}_{-0.06}$	34.18	–5.33
214	10702	1	16.3	1.5	1.85	5.7 ± 0.7	$29.01^{0.05}_{-0.06}$	32.43	–3.43
218	11372	1.1	18.4	1.6	2.33	1.7 ± 0.4	$28.49^{0.09}_{-0.1}$	31.88	–3.39
219	8932	1.9	12.9	0.8	0.85	3.3 ± 0.5	$28.78^{0.06}_{-0.07}$	33.82	–5.05
220	10010	1.4	17.2	1.5	1.93	7.9 ± 0.7	$29.15^{0.04}_{-0.04}$	32.31	–3.15
222	6640	1.1	17.4	1.5	2.08	2.8 ± 0.5	$28.7^{0.06}_{-0.08}$	32.11	–3.41
223	5280	0.8	17.3	1.6	2.15	10.1 ± 1	$29.26^{0.05}_{-0.06}$	32.03	–2.77
225	6106	2.7	12	0.5	0.65	9.2 ± 1	$29.22^{0.04}_{-0.05}$	34.16	–4.94
228	5446	1.3	9.7	0.1	0.2	18.6 ± 1	$29.52^{0.03}_{-0.03}$	34.93	–5.41
229	7483	2.8	13.1	0.8	0.88	2 ± 0.4	$28.55^{0.09}_{-0.1}$	33.75	–5.19
230	9140	1.3	13.4	0.7	0.84	45 ± 2	$29.9^{0.02}_{-0.02}$	33.85	–3.95
231	8408	1.6	15.2	1.1	1.28	8.4 ± 0.7	$29.18^{0.03}_{-0.04}$	32.99	–3.82
233	8654	0.8	14.8	1.1	1.1	3.0 ± 0.5	$28.73^{0.06}_{-0.07}$	33.2	–4.46
234	10871	2.1	14.5	1	1.06	7.1 ± 0.8	$29.11^{0.05}_{-0.05}$	33.29	–4.18
235	6452	0.4	13	0.7	0.79	10.1 ± 1	$29.26^{0.04}_{-0.04}$	33.94	–4.68
236	7864	0.6	12.1	0.6	0.74	43.5 ± 1	$29.89^{0.01}_{-0.01}$	34.03	–4.14
238	8969	1.6	18.9	...	2.49	1.6 ± 0.3	$28.47^{0.08}_{-0.1}$	31.75	–3.28
240	6263	0.8	14.2	0.9	1.01	3.2 ± 0.5	$28.75^{0.06}_{-0.08}$	33.38	–4.63

Table B.1. continued.

X-ray Src	Opt. Id.	Distance arcsec	V mag	$B-V$ mag	$V-I$ mag	f_X (0.3–7.9 keV) 10^{-15} erg s^{-1} cm^{-2}	log L_X erg s^{-1}	log L_{bol} erg s^{-1}	log L_X/L_{bol}
242	7001	0.7	15.7	1.3	1.6	10.5 ± 0.8	$29.27^{0.03}_{-0.03}$	32.69	–3.41
245	5061	2.4	15.4	1.3	1.54	39 ± 2	$29.84^{0.02}_{-0.02}$	32.75	–2.91
246	9202	1	15.2	1.1	1.24	4.4 ± 0.5	$28.9^{0.05}_{-0.06}$	33.04	–4.15
249	8556	4	18.9	1.5	2.57	3.9 ± 0.6	$28.84^{0.06}_{-0.07}$	31.71	–2.87
250	12728	2.6	16.2	1.3	1.58	17 ± 2	$29.5^{0.06}_{-0.06}$	32.7	–3.21
251	10348	1.8	20	...	3	3.8 ± 0.6	$28.83^{0.06}_{-0.07}$	31.54	–2.71
252	7959	0.6	14	1	1.12	17.0 ± 0.9	$29.48^{0.02}_{-0.02}$	33.17	–3.69
254	7505	1.3	19.7	...	2.87	13.3 ± 1	$29.38^{0.03}_{-0.03}$	31.58	–2.21
255	6603	1.2	18.1	1.6	2.36	6.0 ± 0.7	$29.03^{0.05}_{-0.06}$	31.86	–2.83
256	10929	0.5	19.8	...	2.75	1.5 ± 0.4	$28.43^{0.1}_{-0.1}$	31.62	–3.18
257	10863	3.5	12.3	0.6	0.7	18.9 ± 1	$29.53^{0.03}_{-0.03}$	34.09	–4.56
258	4560	4.2	12.4	0.7	0.8	12.1 ± 2	$29.34^{0.06}_{-0.07}$	33.94	–4.6
259	8997	1.1	14.6	1	1.14	34.8 ± 1	$29.79^{0.02}_{-0.02}$	33.16	–3.36
260	7690	2.5	15.2	1.3	1.42	7.1 ± 0.7	$29.1^{0.04}_{-0.04}$	32.87	–3.76
262	6492	0.7	15.9	1.3	1.5	9.8 ± 0.9	$29.25^{0.04}_{-0.04}$	32.8	–3.55
263	9512	0.9	17.9	1.6	2.26	7.3 ± 0.7	$29.12^{0.04}_{-0.04}$	31.93	–2.81
269	10894	1.9	11.9	0.6	-10	20.0 ± 1	$29.55^{0.03}_{-0.03}$	33.97	–4.42
271	9286	0.2	14.2	0.9	1	2.7 ± 0.5	$28.68^{0.07}_{-0.08}$	33.39	–4.71
272	12302	0.3	12	0.5	0.65	21 ± 2	$29.57^{0.04}_{-0.05}$	34.17	–4.6
273	10754	2.3	17.8	1.6	2.38	9.7 ± 0.9	$29.24^{0.04}_{-0.04}$	31.84	–2.6
274	12649	1.8	12.4	0.6	0.74	26 ± 3	$29.67^{0.04}_{-0.05}$	34.03	–4.36
275	8458	1.5	11.5	0.5	0.66	33.3 ± 1	$29.78^{0.01}_{-0.02}$	34.13	–4.36
276	8776	1.2	15.8	1.3	1.48	5.7 ± 0.6	$29.01^{0.04}_{-0.05}$	32.82	–3.81
278	7120	2.8	19.6	...	2.64	2.3 ± 0.5	$28.62^{0.08}_{-0.1}$	31.67	–3.05
279	7553	1.9	13.8	0.8	0.92	9.7 ± 0.8	$29.24^{0.03}_{-0.04}$	33.63	–4.39
282	5989	0.7	20.2	...	2.97	8.8 ± 1	$29.2^{0.05}_{-0.05}$	31.55	–2.36
283	7967	2.5	12.7	0.6	0.74	6.1 ± 0.6	$29.04^{0.04}_{-0.04}$	34.02	–4.98
285	11718	2.9	17.4	1.5	2.04	12.5 ± 1	$29.35^{0.04}_{-0.05}$	32.16	–2.81
289	9061	1.5	17.5	1.7	1.99	2.0 ± 0.4	$28.56^{0.08}_{-0.1}$	32.21	–3.64
290	8099	0.2	12.2	0.6	0.68	28.5 ± 1	$29.71^{0.02}_{-0.02}$	34.11	–4.4
295	9054	3.3	12.8	0.7	0.84	42.0 ± 1	$29.88^{0.01}_{-0.01}$	33.85	–3.98
298	7104	1	12.7	0.6	0.75	11.9 ± 0.9	$29.33^{0.03}_{-0.03}$	34.01	–4.69
300	7667	0.8	9.9	0.2	0.25	25.2 ± 1	$29.65^{0.02}_{-0.02}$	34.8	–5.15
302	8737	0.8	14.8	1	1.12	1.9 ± 0.4	$28.54^{0.08}_{-0.09}$	33.18	–4.63
304	10143	1.8	19.9	...	3.01	3.5 ± 0.6	$28.8^{0.07}_{-0.08}$	31.54	–2.74
305	6268	0.3	14.9	1.1	1.2	18.5 ± 1	$29.52^{0.03}_{-0.03}$	33.09	–3.57
310	11782	1.6	14.6	1	1.16	1.9 ± 0.7	$28.53^{0.1}_{-0.2}$	33.14	–4.61
311	8332	1.1	9.7	0.2	0.28	8.9 ± 0.7	$29.2^{0.03}_{-0.04}$	34.76	–5.56
312	10191	2	19.4	...	3.06	2.7 ± 0.5	$28.68^{0.07}_{-0.08}$	31.52	–2.84
313	5024	0.6	16.3	1.3	1.66	18 ± 2	$29.5^{0.04}_{-0.04}$	32.64	–3.14
315	6847	3.4	18.9	...	2.43	2.8 ± 0.6	$28.7^{0.08}_{-0.1}$	31.8	–3.1
320	11451	1.8	19.4	...	2.68	2.4 ± 0.6	$28.63^{0.09}_{-0.1}$	31.65	–3.02
322	7203	1.9	19.6	...	2.62	4.9 ± 0.7	$28.94^{0.05}_{-0.06}$	31.69	–2.74
323	10046	1.3	14.8	1	1.14	46.8 ± 1	$29.92^{0.01}_{-0.01}$	33.16	–3.23
327	12874	1.7	13.5	0.9	1.05	29 ± 5	$29.71^{0.07}_{-0.08}$	33.31	–3.6
328	11153	1.5	20.1	...	2.8	5.8 ± 0.8	$29.02^{0.06}_{-0.07}$	31.6	–2.59
331	11485	1	14.8	1	1.21	25 ± 2	$29.65^{0.03}_{-0.03}$	33.09	–3.44
332	7622	6.9	17.2	1.5	1.91	16.1 ± 1	$29.46^{0.03}_{-0.03}$	32.35	–2.89
337	7420	2.3	17.8	1.6	2.12	4.7 ± 0.6	$28.92^{0.06}_{-0.06}$	32.07	–3.15
338	6508	2	18.4	1.6	2.6	5.9 ± 0.9	$29.03^{0.06}_{-0.07}$	31.7	–2.67
339	6676	1	14.3	0.9	1.01	2.4 ± 0.5	$28.64^{0.08}_{-0.1}$	33.38	–4.74
342	11970	2	10.8	0.3	0.4	28 ± 2	$29.7^{0.03}_{-0.03}$	34.53	–4.83
343	8529	1	12.3	0.6	0.71	31.8 ± 1	$29.76^{0.02}_{-0.02}$	34.07	–4.32
346	8886	4.3	9.7	0.1	0.13	55.2 ± 2	$30^{0.02}_{-0.02}$	35.08	–5.08
347	9328	4.3	12.2	0.6	0.67	18.7 ± 1	$29.52^{0.03}_{-0.03}$	34.12	–4.59
349	9572	0.6	19.1	...	2.87	2.0 ± 0.4	$28.56^{0.08}_{-0.09}$	31.58	–3.02
350	8536	0.9	12.9	0.7	0.76	3.0 ± 0.5	$28.72^{0.07}_{-0.09}$	34	–5.27
351	10330	0.4	19.6	...	2.72	2.5 ± 0.5	$28.65^{0.09}_{-0.1}$	31.63	–2.98
353	10695	0.9	16.8	1.5	1.78	7.9 ± 1	$29.15^{0.05}_{-0.06}$	32.52	–3.37

Table B.1. continued.

X-ray Src	Opt. Id.	Distance	V	$B-V$	$V-I$	f_X (0.3–7.9 keV)	log L_X	log L_{bol}	log L_X/L_{bol}
		arcsec	mag	mag	mag	10^{-15} erg s^{-1} cm^{-2}	erg s^{-1}	erg s^{-1}	
355	11867	3.7	12.6	0.6	0.73	7.6 ± 1	$29.13^{0.07}_{-0.08}$	34.05	–4.91
358	7322	3.4	15	1.1	1.14	7.0 ± 0.9	$29.1^{0.05}_{-0.06}$	33.16	–4.07
360	10047	1.9	18.5	1.7	2.34	5.3 ± 0.7	$28.98^{0.05}_{-0.06}$	31.87	–2.89
362	5836	1.4	19.6	...	3.07	4.6 ± 0.9	$28.92^{0.07}_{-0.09}$	31.52	–2.6
363	6029	0.7	12.2	0.7	0.77	49 ± 2	$29.94^{0.02}_{-0.02}$	33.98	–4.04
364	6180	2.2	18.6	1.6	2.71	4.7 ± 0.7	$28.93^{0.06}_{-0.07}$	31.64	–2.71
367	7595	1	12.6	0.6	0.7	12.4 ± 0.9	$29.35^{0.03}_{-0.03}$	34.08	–4.74
370	10605	1.7	13.6	0.8	0.89	4.5 ± 0.7	$28.9^{0.06}_{-0.07}$	33.73	–4.83
371	9446	2.4	13.6	0.8	0.85	5.0 ± 0.9	$28.95^{0.07}_{-0.08}$	33.82	–4.87
372	8634	1	14.5	0.9	1.12	58 ± 2	$30.02^{0.01}_{-0.01}$	33.18	–3.16
375	12118	2	14.3	0.9	1.08	9 ± 2	$29.19^{0.08}_{-0.1}$	33.24	–4.05
384	11132	1.2	17.4	1.5	2.01	12.2 ± 1	$29.34^{0.05}_{-0.05}$	32.19	–2.85
387	5312	4.3	18	1.5	2.24	6.7 ± 1	$29.08^{0.08}_{-0.1}$	31.94	–2.86
388	9453	0.8	17.7	1.6	2.1	4.7 ± 0.7	$28.93^{0.06}_{-0.07}$	32.1	–3.17
390	9241	1.8	9.6	0.1	0.08	4.0 ± 0.7	$28.86^{0.07}_{-0.09}$	35.17	–6.32
391	6577	2.1	19.4	...	2.66	3.5 ± 0.7	$28.8^{0.08}_{-0.1}$	31.66	–2.86
396	6070	2.7	15	1.1	1.2	19 ± 2	$29.53^{0.04}_{-0.04}$	33.09	–3.56
398	8261	2.8	12	0.5	0.6	16.1 ± 1	$29.46^{0.03}_{-0.03}$	34.28	–4.82
400	7028	1.7	18.7	1.6	2.46	4.8 ± 0.9	$28.94^{0.08}_{-0.09}$	31.77	–2.83
402	6650	1.1	18.1	1.7	2.18	13.1 ± 1	$29.37^{0.04}_{-0.05}$	31.98	–2.61
403	7918	2.1	18.8	1.6	2.39	7.9 ± 1	$29.15^{0.05}_{-0.06}$	31.84	–2.69
404	10884	2	19.1	1.6	2.65	4.2 ± 0.8	$28.87^{0.08}_{-0.1}$	31.67	–2.8
405	9079	6.5	20.3	...	3	5.3 ± 0.8	$28.97^{0.06}_{-0.07}$	31.55	–2.57
408	8242	4.3	17.3	1.5	1.89	2.0 ± 0.5	$28.55^{0.1}_{-0.1}$	32.37	–3.83
409	8935	0.8	10.6	0.3	0.39	16.7 ± 1	$29.48^{0.03}_{-0.04}$	34.56	–5.08
412	11982	1.9	19.1	...	2.56	5.1 ± 1	$28.96^{0.1}_{-0.1}$	31.72	–2.76
414	8660	1.9	12.4	0.6	0.67	27 ± 2	$29.69^{0.02}_{-0.03}$	34.12	–4.43
416	9727	5.6	19.8	...	2.9	5.1 ± 1	$28.96^{0.08}_{-0.1}$	31.57	–2.62
417	8989	1.8	18.6	1.5	2.42	3.8 ± 0.8	$28.83^{0.08}_{-0.1}$	31.81	–2.98
418	10902	1.7	18.1	1.6	2.25	5.6 ± 1	$29^{0.08}_{-0.09}$	31.94	–2.94
419	10293	0.5	15.5	1.2	1.31	5.5 ± 0.9	$28.99^{0.07}_{-0.08}$	32.95	–3.96
425	10040	3.3	14.9	1	1.17	40 ± 3	$29.86^{0.03}_{-0.03}$	33.13	–3.27
426	9882	2.2	9.8	0.2	0.24	13.0 ± 0.8	$29.37^{0.03}_{-0.03}$	34.83	–5.47
428	7596	6.8	16.2	1.4	1.65	19 ± 2	$29.54^{0.04}_{-0.04}$	32.65	–3.11
432	8453	3.1	15.9	1.3	1.47	3.9 ± 0.9	$28.85^{0.09}_{-0.1}$	32.82	–3.97
434	9835	1	14.8	1	1.13	51 ± 2	$29.96^{0.02}_{-0.02}$	33.17	–3.21
436	8397	1	20	...	3.08	2.9 ± 0.7	$28.71^{0.09}_{-0.1}$	31.52	–2.81
437	7941	1.1	13.1	0.7	0.77	8.0 ± 1	$29.15^{0.06}_{-0.07}$	33.98	–4.83
439	10817	0.7	11.9	0.5	0.65	375 ± 10	$30.83^{0.02}_{-0.02}$	34.16	–3.33
442	10957	3.4	17.7	1.6	2.31	4.8 ± 1	$28.93^{0.09}_{-0.1}$	31.9	–2.97
446	8999	0.8	13.4	0.7	0.85	4.6 ± 1	$28.92^{0.09}_{-0.1}$	33.82	–4.9
453	5957	5	14.6	1	1.08	41 ± 6	$29.87^{0.06}_{-0.07}$	33.25	–3.39
455	10434	2.5	18.1	1.6	2.29	6.9 ± 1	$29.09^{0.09}_{-0.1}$	31.91	–2.82
456	9486	0.4	12.6	0.8	0.86	39 ± 3	$29.85^{0.03}_{-0.03}$	33.79	–3.94
4	8665	1.9	13.1	0.7	0.83	7 ± 1	$29.1^{0.07}_{-0.09}$	33.87	–4.77
4	8675	5.1	13.2	...	0.84	7 ± 1	$29.1^{0.07}_{-0.09}$	33.86	–4.75
36	4750	0.6	12.3	0.5	0.59	9 ± 2	$29.2^{0.08}_{-0.1}$	34.29	–5.09
36	4760	3.4	13.1	0.7	0.83	9 ± 2	$29.2^{0.08}_{-0.1}$	33.86	–4.66
85	8641	3.1	14.1	1.1	1.14	34.0 ± 1	$29.78^{0.01}_{-0.01}$	33.16	–3.37
85	8645	1.4	14.1	1.1	1.14	34.0 ± 1	$29.78^{0.01}_{-0.01}$	33.16	–3.37
105	8967	1.5	14.8	1	1.14	36 ± 2	$29.81^{0.02}_{-0.02}$	33.16	–3.34
303	5835	4.1	13.3	...	0.84	5.8 ± 0.6	$29.02^{0.04}_{-0.04}$	33.85	–4.83
303	5862	1.4	13.3	0.7	0.84	5.8 ± 0.6	$29.02^{0.04}_{-0.04}$	33.84	–4.82
385	5887	2.2	13.7	0.9	0.99	9.8 ± 1	$29.25^{0.05}_{-0.06}$	33.42	–4.17
186	15496	2	8.4	0	...	31 ± 2	$30.07^{0.01}_{-0.01}$	36.35	–6.28
193	15499	2.5	9.3	0.1	...	16.9 ± 1	$29.48^{0.03}_{-0.03}$	35.03	–5.55
89	15500	3.3	8.8	0.1	...	18.6 ± 1	$29.52^{0.03}_{-0.03}$	35.45	–5.92
423	15501	0.5	8.4	0	...	18 ± 2	$29.51^{0.04}_{-0.05}$	36.75	–7.24
192	15503	1.3	8.9	0.1	...	8.6 ± 0.8	$29.19^{0.04}_{-0.04}$	35.27	–6.08

Table B.1. continued.

X-ray Src	Opt. Id.	Distance arcsec	V mag	$B-V$ mag	$V-I$ mag	f_X (0.3–7.9 keV) 10^{-15} erg s^{-1} cm^{-2}	log L_X erg s^{-1}	log L_{bol} erg s^{-1}	log L_X/L_{bol}
132	15504	0.6	9.5	0.2	...	19.6 ± 1	$29.55^{0.02}_{-0.02}$	34.77	–5.22
141	15506	1.9	8	0	...	29.5 ± 1	$29.67^{0.02}_{-0.03}$	36.9	–7.23
141	15507	3.9	7.2	0	...	29.5 ± 1	$29.67^{0.02}_{-0.03}$	36.45	–6.78
176	15509	1.7	5.8	–0.1	...	102 ± 2	$29.63^{0.04}_{-0.05}$	...	...
399	15510	4.7	9.5	0.1	...	131 ± 4	$30.37^{0.01}_{-0.01}$	35.27	–4.9
188	15512	0.9	9.1	0	...	41 ± 2	$30.61^{0.004}_{-0.004}$	36.21	–5.6
232	15540	0.6	8.4	0.1	...	4.2 ± 0.6	$28.88^{0.06}_{-0.06}$	35.45	–6.57

Appendix C: X-ray upper limits of NGC 2516 stars

Table C.1. X-ray undetected stars of NGC 2516. Columns report: identifier from Jeffries et al. (2001), V, $B-V$, $V-I$, exposure time (ks), upper limit to rate (ct/ks), flux and luminosities in the 0.3–7.9 keV band, log $L_{\rm bol}$ and the ratio log $L_{\rm X}/L_{\rm bol}$.

Opt. Id.	V mag	$B-V$ mag	$V-I$ mag	Time ks	Limit rate ct ks^{-1}	Lim. log $f_{\rm X}$ erg s^{-1} cm^{-2}	Lim. log $L_{\rm X}$ erg s^{-1}	log $L_{\rm bol}$ erg s^{-1}	log $L_{\rm X}/L_{\rm bol}$
3680	17.238	1.537	1.909	11.28	≤1.321	≤–13.9	≤29.35	32.34	≤–2.99
3748	15.753	1.211	1.446	11.28	1.443	–13.86	29.39	32.84	–3.45
3777	20.005	...	3.113	11.34	1.439	–13.86	29.39	31.51	–2.12
3891	17.183	1.564	2.022	11.49	1.324	–13.9	29.35	32.18	–2.83
4069	19.661	...	2.964	11.73	1.35	–13.89	29.36	31.55	–2.19
4072	18.981	...	2.47	12.14	1.253	–13.92	29.33	31.76	–2.43
4146	20.693	...	3.361	27.16	1.077	–13.99	29.26	31.42	–2.16
4187	14.492	1.112	1.214	23.01	0.87	–14.08	29.17	33.08	–3.91
4229	14.797	1.114	1.145	22.38	0.89	–14.07	29.18	33.15	–3.97
4254	19.564	...	2.835	22.32	0.859	–14.09	29.17	31.59	–2.42
4322	19.858	...	2.795	28.66	0.787	–14.13	29.13	31.6	–2.47
4364	19.245	1.601	2.884	14.12	1.44	–13.86	29.39	31.58	–2.19
4397	18.385	1.646	2.357	29.49	0.842	–14.1	29.16	31.86	–2.7
4432	18.438	1.565	2.374	19.51	1.205	–13.94	29.31	31.85	–2.54
4448	14.674	1.126	1.277	33.96	0.728	–14.16	29.09	33	–3.91
4473	20.164	...	3.155	25.8	0.858	–14.09	29.16	31.49	–2.33
4479	19.411	...	2.572	58.82	0.582	–14.26	29	31.71	–2.71
4530	20.774	...	3.142	36.33	0.825	–14.11	29.15	31.5	–2.35
4574	13.02	0.671	0.762	14.56	1.378	–13.88	29.37	34	–4.63
4647	19.043	...	2.529	27.35	1.063	–14	29.26	31.73	–2.47
4648	20.739	...	3.128	17.06	1.311	–13.9	29.35	31.5	–2.15
4718	19.27	...	2.784	17.09	1.251	–13.92	29.33	31.61	–2.28
4727	19.783	...	2.793	64.65	0.474	–14.35	28.91	31.6	–2.69
4808	19.942	...	2.706	74.21	0.485	–14.34	28.92	31.64	–2.72
4836	18.702	...	2.488	32.09	0.757	–14.14	29.11	31.75	–2.64
4840	10.609	0.256	0.321	28.45	0.833	–14.1	29.15	34.67	–5.52
4842	11.243	0.397	0.478	26.09	0.872	–14.08	29.17	34.45	–5.28
4855	14.613	1.106	1.206	67.52	0.507	–14.32	28.94	33.09	–4.15
4889	11.651	0.449	0.58	31.99	0.771	–14.14	29.12	34.31	–5.19
4914	13.541	0.768	0.853	23.79	0.7	–14.18	29.08	33.81	–4.73
4936	20.675	...	3.086	49.89	0.527	–14.3	28.95	31.52	–2.57
5010	18.72	1.547	2.481	88.93	0.371	–14.45	28.8	31.75	–2.95
5018	18.906	...	2.531	8.79	1.67	–13.8	29.45	31.73	–2.28
5079	20.711	...	3.148	127.74	0.342	–14.49	28.76	31.49	–2.73
5088	19.493	...	2.611	44.63	0.624	–14.23	29.03	31.69	–2.66
5107	12.297	0.535	0.631	8.77	1.342	–13.89	29.36	34.21	–4.85
5144	18.934	1.577	2.726	45.38	0.759	–14.14	29.11	31.63	–2.52
5175	20.029	...	2.839	141.43	0.301	–14.54	28.71	31.59	–2.88
5193	19.03	...	2.647	118.63	0.338	–14.49	28.76	31.67	–2.91
5243	19.748	...	3.005	62.38	0.569	–14.27	28.99	31.54	–2.55
5262	15.244	1.069	1.146	155.23	0.274	–14.58	28.67	33.15	–4.48
5285	19.306	...	2.663	51.08	0.697	–14.18	29.07	31.66	–2.59
5363	20.554	...	3.178	46.97	0.681	–14.19	29.06	31.48	–2.42
5429	20.192	...	3.096	69.81	0.4	–14.42	28.83	31.51	–2.68
5499	15.227	1.124	1.222	54.36	0.632	–14.22	29.03	33.07	–4.04
5509	18.963	1.729	2.534	160.54	0.316	–14.52	28.73	31.73	–3
5526	16.943	1.488	1.842	151.82	0.301	–14.54	28.71	32.45	–3.74
5528	18.837	1.689	2.54	18.55	0.866	–14.08	29.17	31.72	–2.55
5530	15.661	1.215	1.358	140.48	0.322	–14.51	28.74	32.91	–4.17
5533	19.636	1.699	2.786	82.61	0.398	–14.42	28.83	31.61	–2.78
5536	13.126	0.697	0.818	9.24	1.355	–13.89	29.36	33.89	–4.53
5573	20.124	...	3.156	147.94	0.284	–14.57	28.68	31.49	–2.81
5581	11.247	0.366	0.456	60.07	0.471	–14.35	28.9	34.48	–5.58
5626	11.066	0.507	0.617	132.89	0.326	–14.51	28.74	34.24	–5.5
5631	14.999	1.065	1.201	156.81	0.272	–14.59	28.67	33.09	–4.42
5678	14.637	1.027	1.131	51.29	0.644	–14.21	29.04	33.17	–4.13
5685	21.043	...	3.063	29.07	0.778	–14.13	29.12	31.52	–2.4

Table C.1. continued.

Opt. Id.	V mag	$B-V$ mag	$V-I$ mag	Time ks	Limit rate ct ks^{-1}	Lim. log f_X erg s^{-1} cm^{-2}	Lim. log L_X erg s^{-1}	log L_{bol} erg s^{-1}	log L_X/L_{bol}
5741	17.926	1.508	2.169	17.46	0.776	–14.13	29.12	32	–2.88
5785	20.01	...	2.831	116.58	0.365	–14.46	28.79	31.59	–2.8
5843	17.878	1.456	2.16	93.23	0.4	–14.42	28.83	32.01	–3.18
5849	16.713	1.542	1.965	14.99	0.848	–14.09	29.16	32.23	–3.07
5871	18.767	1.608	2.38	27.94	0.898	–14.07	29.18	31.84	–2.66
5875	15.428	1.141	1.232	178.22	0.685	–14.19	29.07	33.06	–3.99
5876	18.107	1.527	2.42	186.44	0.829	–14.1	29.15	31.81	–2.66
5878	18.623	1.642	2.47	46.57	1.224	–13.93	29.32	31.76	–2.44
5882	19.11	...	2.481	174.73	1.229	–13.93	29.32	31.75	–2.43
5904	15.043	1.086	1.158	27.8	0.94	–14.05	29.2	33.14	–3.94
5911	14.592	1.016	1.096	187.57	0.531	–14.3	28.96	33.22	–4.26
5972	18.458	1.6	2.341	42.93	0.563	–14.27	28.98	31.87	–2.89
5991	18.463	1.618	2.327	131.48	0.344	–14.49	28.77	31.88	–3.11
6027	12.151	0.632	0.766	56.89	0.493	–14.33	28.92	33.99	–5.07
6036	12.078	0.562	0.699	54.06	0.464	–14.36	28.9	34.08	–5.18
6044	21.234	...	3.231	94.48	0.46	–14.36	28.89	31.46	–2.57
6049	14.701	1.014	1.094	157.18	0.305	–14.54	28.72	33.22	–4.5
6057	20.197	...	2.927	56.04	0.61	–14.24	29.02	31.57	–2.55
6077	20.937	...	3.17	67.71	0.513	–14.31	28.94	31.49	–2.55
6095	16.668	1.467	1.733	156.94	0.313	–14.53	28.73	32.57	–3.84
6096	12.053	0.515	0.619	156.54	0.288	–14.56	28.69	34.23	–5.54
6112	18.809	1.563	2.522	38.29	0.563	–14.27	28.98	31.73	–2.75
6152	19.891	...	2.987	157.77	0.315	–14.52	28.73	31.55	–2.82
6177	10.2	0.181	0.188	62.65	0.467	–14.35	28.9	34.84	–5.94
6204	17.645	1.586	2.169	159.83	0.297	–14.55	28.7	32	–3.3
6209	14.907	1.096	1.185	45.8	0.49	–14.33	28.92	33.11	–4.19
6222	14.951	...	1.185	46.02	0.488	–14.33	28.92	33.11	–4.19
6238	19.34	1.605	2.721	202.96	0.231	–14.66	28.59	31.63	–3.04
6264	19.866	...	2.731	189.93	0.257	–14.61	28.64	31.63	–2.99
6289	19.175	...	2.858	107.31	0.449	–14.37	28.88	31.59	–2.71
6297	19.032	1.703	2.463	16.37	1.068	–13.99	29.26	31.77	–2.51
6301	13.01	0.64	0.73	64.38	0.483	–14.34	28.91	34.04	–5.13
6323	19.629	...	2.834	103.93	0.403	–14.42	28.84	31.59	–2.75
6377	11.742	0.463	0.559	149.97	1.145	–13.96	29.29	34.35	–5.06
6402	20.505	...	2.973	204.72	0.249	–14.63	28.63	31.55	–2.92
6445	19.745	...	2.752	170.95	0.279	–14.58	28.68	31.61	–2.93
6446	11.37	0.386	0.474	139.18	0.361	–14.47	28.79	34.46	–5.67
6501	12.812	0.703	0.846	219.17	0.231	–14.66	28.59	33.83	–5.24
6575	9.913	0.2	0.251	211.36	1.784	–13.77	29.48	34.79	–5.31
6594	20.29	...	2.966	178.37	0.253	–14.62	28.63	31.55	–2.92
6691	20.334	...	2.981	75.8	0.411	–14.41	28.85	31.55	–2.7
6705	13.968	1.022	1.108	213.44	0.215	–14.69	28.56	33.19	–4.63
6724	14.009	1.043	1.112	193.66	0.236	–14.65	28.6	33.18	–4.58
6725	18.357	1.556	2.367	57.17	0.522	–14.3	28.95	31.85	–2.9
6771	19.202	...	2.517	230.76	0.194	–14.73	28.52	31.73	–3.21
6796	10.26	0.194	0.223	32.95	1.273	–13.92	29.34	34.81	–5.47
6880	13.293	0.814	0.875	210.01	0.207	–14.71	28.55	33.76	–5.21
6912	10.875	0.318	0.328	206.25	0.229	–14.66	28.59	34.53	–5.94
6940	16.898	1.593	1.924	230.33	0.198	–14.73	28.53	32.32	–3.79
6942	11.17	0.355	0.422	133.14	0.3	–14.55	28.71	34.46	–5.75
6949	11.25	0.376	0.456	211.72	0.216	–14.69	28.57	34.48	–5.91
6963	15.28	1.14	1.234	213.08	0.246	–14.63	28.62	33.05	–4.43
6965	17.862	1.539	2.498	122.97	0.279	–14.58	28.68	31.74	–3.06
6996	18.703	...	2.471	203.15	1.711	–13.79	29.46	31.76	–2.3
7041	10.198	0.159	0.163	216.32	0.207	–14.71	28.55	34.9	–6.35
7113	20.25	...	3.182	48.67	0.7	–14.18	29.08	31.48	–2.4
7154	17.875	1.626	2.425	232.26	0.246	–14.63	28.62	31.8	–3.18
7189	11.753	0.499	0.625	229.62	0.216	–14.69	28.56	34.22	–5.66
7206	10.638	0.261	0.332	262.95	0.192	–14.74	28.51	34.66	–6.15

Table C.1. continued.

Opt. Id.	V mag	$B-V$ mag	$V-I$ mag	Time ks	Limit rate ct ks^{-1}	Lim. log f_X erg s^{-1} cm^{-2}	Lim. log L_X erg s^{-1}	log L_{bol} erg s^{-1}	log L_X/L_{bol}
7207	14.723	1.018	1.103	65.64	0.563	–14.27	28.98	33.2	–4.22
7259	14.371	0.934	0.992	15.19	0.856	–14.09	29.16	33.4	–4.24
7260	18.957	...	2.736	209.99	0.721	–14.16	29.09	31.62	–2.53
7335	11.216	...	0.451	104.5	0.316	–14.52	28.73	34.48	–5.75
7347	11.195	0.365	0.446	105.71	0.32	–14.52	28.74	34.45	–5.71
7352	16.28	...	1.635	109.94	2.474	–13.63	29.62	32.66	–3.04
7419	18.702	...	2.568	217.6	1.493	–13.85	29.41	31.71	–2.3
7442	16.904	1.464	1.822	44.8	0.563	–14.27	28.98	32.47	–3.49
7443	10.91	0.318	0.366	194.14	0.86	–14.09	29.17	34.53	–5.36
7454	14.362	0.931	1.023	78.75	0.46	–14.36	28.89	33.36	–4.47
7480	17.322	1.483	2.004	15.33	0.912	–14.06	29.19	32.19	–3
7504	20.392	...	2.879	133.84	0.415	–14.4	28.85	31.58	–2.73
7542	19.648	...	2.692	15.69	1.013	–14.02	29.24	31.65	–2.41
7559	21.467	...	3.276	210.15	1.325	–13.9	29.35	31.45	–2.1
7590	13.99	0.885	0.996	228.4	1.497	–13.85	29.41	33.4	–3.99
7599	20	...	2.949	44.24	0.551	–14.28	28.97	31.56	–2.59
7613	18.543	1.707	2.349	15.1	0.942	–14.05	29.21	31.87	–2.66
7628	19.279	...	2.658	116.43	0.253	–14.62	28.63	31.67	–3.04
7666	20.296	...	3.115	235.26	1.515	–13.84	29.41	31.51	–2.1
7721	14.861	1.048	1.152	49.02	0.532	–14.3	28.96	33.15	–4.19
7734	19.465	...	2.648	106.96	0.362	–14.46	28.79	31.67	–2.88
7771	15.112	1.16	1.166	142.76	0.31	–14.53	28.72	33.13	–4.41
7788	14.832	1.11	1.269	229.83	0.199	–14.72	28.53	33.01	–4.48
7806	16.29	1.367	1.597	51.76	0.675	–14.19	29.06	32.69	–3.63
7813	14.605	0.984	1.086	23.41	0.889	–14.07	29.18	33.24	–4.06
7838	10.415	0.379	0.47	249.04	0.181	–14.76	28.49	34.46	–5.97
7842	11.111	0.353	0.4	59.06	0.504	–14.32	28.93	34.46	–5.53
7900	11.254	0.477	0.614	61.21	0.578	–14.26	28.99	34.24	–5.25
7937	15.359	1.171	1.265	215.48	0.26	–14.61	28.65	33.01	–4.36
7984	18.687	1.625	2.381	51.3	0.57	–14.27	28.99	31.84	–2.85
7985	17.36	1.511	2.279	19.28	0.87	–14.08	29.17	31.92	–2.75
8031	18.989	...	2.742	196.64	0.235	–14.65	28.6	31.62	–3.02
8047	16.116	1.356	1.606	253.51	3.347	–13.5	29.76	32.68	–2.92
8055	14.951	1.077	1.136	289.12	0.175	–14.78	28.48	33.16	–4.68
8058	10.725	0.328	0.445	297.54	0.391	–14.43	28.82	34.5	–5.68
8132	15.717	1.201	1.324	118.71	0.388	–14.43	28.82	32.94	–4.12
8138	19.128	...	2.508	297.25	0.527	–14.3	28.95	31.74	–2.79
8166	15.164	1.101	1.217	276.94	0.177	–14.77	28.48	33.07	–4.59
8219	19.204	...	2.815	60.52	0.603	–14.24	29.01	31.6	–2.59
8256	13.507	0.902	0.998	59.23	2.821	–13.57	29.68	33.39	–3.71
8262	14.215	0.95	0.982	186.6	1.693	–13.79	29.46	33.44	–3.98
8289	20.446	...	2.979	83.79	0.435	–14.38	28.87	31.55	–2.68
8298	14.007	1.061	1.146	117.46	0.389	–14.43	28.82	33.15	–4.33
8313	10.439	0.275	0.285	166.09	0.248	–14.63	28.63	34.63	–6
8320	14.821	1.055	1.164	15.04	0.974	–14.03	29.22	33.13	–3.91
8340	10.117	0.149	0.168	295.59	0.341	–14.49	28.76	34.92	–6.16
8359	18.162	1.57	2.217	107.84	0.405	–14.42	28.84	31.96	–3.12
8385	19.621	...	2.866	15.08	0.974	–14.03	29.22	31.58	–2.36
8391	20.527	...	2.912	245.82	0.189	–14.75	28.51	31.57	–3.06
8401	18.855	...	2.578	145.76	0.323	–14.51	28.74	31.71	–2.97
8465	13.291	0.696	0.812	136.01	0.343	–14.49	28.77	33.91	–5.14
8509	18.401	1.57	2.418	122.89	0.304	–14.54	28.71	31.81	–3.1
8524	10.972	0.334	0.398	293.83	0.163	–14.81	28.44	34.49	–6.05
8531	15.479	1.211	1.299	229.17	0.207	–14.71	28.55	32.96	–4.41
8591	18.214	1.604	2.617	237.27	0.205	–14.71	28.54	31.69	–3.15
8678	18.24	1.474	2.338	126.88	1.385	–13.88	29.37	31.88	–2.51
8714	19.74	...	2.679	251.88	0.186	–14.75	28.5	31.65	–3.15
8727	19.639	...	2.713	295.11	0.161	–14.82	28.44	31.64	–3.2
8801	19.95	...	2.766	201.11	0.222	–14.68	28.58	31.61	–3.03

Table C.1. continued.

Opt. Id.	V mag	$B-V$ mag	$V-I$ mag	Time ks	Limit rate ct ks^{-1}	Lim. log f_X erg s^{-1} cm^{-2}	Lim. log L_X erg s^{-1}	log L_{bol} erg s^{-1}	log L_X/L_{bol}
8827	14.35	1.001	1.059	163.56	0.267	–14.6	28.66	33.29	–4.63
8917	10.379	0.186	0.204	164.33	0.274	–14.58	28.67	34.83	–6.16
8920	11.682	0.475	0.606	236.6	0.234	–14.65	28.6	34.26	–5.66
8923	13.974	1.031	1.099	255.74	3.802	–13.44	29.81	33.21	–3.4
8949	15.842	...	1.539	131.64	0.397	–14.42	28.83	32.75	–3.92
8950	17.781	1.461	2.169	14.89	1.064	–14	29.26	32	–2.74
9058	20.699	...	2.972	247.2	0.232	–14.66	28.6	31.55	–2.95
9088	21.486	...	3.348	16.75	0.899	–14.07	29.19	31.42	–2.23
9146	14.125	1.041	1.12	225.17	0.202	–14.72	28.54	33.18	–4.64
9153	19.193	...	2.589	293.99	0.462	–14.36	28.9	31.7	–2.8
9197	13.421	0.727	0.845	16.13	0.892	–14.07	29.18	33.83	–4.65
9214	15.281	1.146	1.255	99.3	0.335	–14.5	28.76	33.03	–4.27
9243	10.85	0.279	0.304	90.36	0.364	–14.46	28.79	34.62	–5.83
9259	19.302	1.678	2.612	159.55	0.296	–14.55	28.7	31.69	–2.99
9270	20.123	...	2.838	169.35	0.303	–14.54	28.71	31.59	–2.88
9361	13.59	0.779	0.889	241.27	1.967	–13.73	29.52	33.73	–4.21
9402	17.733	1.564	2.123	269.45	1.09	–13.98	29.27	32.06	–2.79
9415	18.137	1.481	2.449	259.27	1.09	–13.98	29.27	31.78	–2.51
9427	20.279	...	3.135	70.06	0.565	–14.27	28.98	31.5	–2.52
9459	14.932	1.026	1.147	51.49	0.556	–14.28	28.98	33.15	–4.17
9475	13.699	0.832	0.964	225.43	0.206	–14.71	28.55	33.5	–4.95
9513	14.475	0.953	1.03	198.89	0.282	–14.57	28.68	33.34	–4.66
9590	17.851	1.551	2.167	29.83	1.121	–13.97	29.28	32	–2.72
9596	15.519	1.144	1.27	247.44	0.204	–14.71	28.54	33.01	–4.47
9600	11.714	0.41	0.59	13.61	1.186	–13.95	29.31	34.29	–4.98
9655	14.802	1.034	1.124	204.62	0.61	–14.24	29.02	33.17	–4.15
9659	11.448	0.408	0.56	245.94	0.199	–14.72	28.53	34.34	–5.81
9682	12.308	0.551	0.676	7.88	1.79	–13.77	29.48	34.11	–4.63
9684	15.167	1.05	1.126	115.16	0.344	–14.49	28.77	33.17	–4.4
9700	19.092	...	2.577	129.68	0.331	–14.5	28.75	31.71	–2.96
9707	15.114	1.146	1.239	37.07	0.686	–14.19	29.07	33.05	–3.98
9791	11.231	0.381	0.459	199.94	0.256	–14.61	28.64	34.47	–5.83
9811	10.806	0.28	0.312	195.03	0.211	–14.7	28.56	34.62	–6.06
9875	15.234	1.048	1.136	270.83	0.167	–14.8	28.45	33.16	–4.71
9878	15.461	1.17	1.237	16.83	0.809	–14.11	29.14	33.05	–3.91
9885	17.896	1.536	2.222	122.5	0.309	–14.53	28.72	31.96	–3.24
9939	19.167	...	2.858	258.03	0.187	–14.75	28.5	31.59	–3.09
9959	17.183	1.62	2.077	219.69	0.244	–14.63	28.62	32.12	–3.5
9961	20.698	...	3.355	264.82	0.192	–14.74	28.51	31.42	–2.91
10077	19.089	...	2.804	228.61	7.577	–13.14	30.11	31.6	–1.49
10129	16.482	1.422	1.653	180.47	0.242	–14.64	28.62	32.65	–4.03
10132	14.85	1.157	1.221	233.22	0.179	–14.77	28.48	33.07	–4.59
10152	13.035	0.711	0.845	173.71	0.273	–14.59	28.67	33.83	–5.16
10162	17.617	1.584	2.042	243.92	0.192	–14.74	28.52	32.15	–3.63
10165	19.103	...	2.562	50.17	0.623	–14.23	29.03	31.71	–2.68
10281	13.426	0.748	0.824	64.09	0.464	–14.36	28.9	33.88	–4.98
10284	15.306	1.182	1.274	53.28	0.596	–14.25	29.01	33	–3.99
10285	19.222	1.595	2.488	50.43	0.622	–14.23	29.03	31.75	–2.72
10298	20.556	...	3.386	224.53	0.206	–14.71	28.55	31.41	–2.86
10301	11.534	0.444	0.542	167.96	0.27	–14.59	28.66	34.37	–5.71
10365	15.874	1.255	1.467	187.65	0.846	–14.09	29.16	32.82	–3.66
10368	15.475	1.245	1.311	43.56	0.545	–14.29	28.97	32.95	–3.98
10370	18.136	1.65	2.603	51.65	0.607	–14.24	29.01	31.69	–2.68
10383	17.736	1.512	2.152	13.09	1.29	–13.91	29.34	32.02	–2.68
10398	17.395	1.481	2.216	61.82	0.551	–14.28	28.97	31.96	–2.99
10401	18.516	1.51	2.42	59.9	0.565	–14.27	28.98	31.81	–2.83
10496	19.516	...	2.577	13.01	1.239	–13.93	29.32	31.71	–2.39
10503	17.023	1.502	1.879	44.1	0.542	–14.29	28.96	32.39	–3.43
10505	20.229	...	2.829	16.01	2.257	–13.67	29.58	31.59	–2.01

Table C.1. continued.

Opt. Id.	V mag	$B-V$ mag	$V-I$ mag	Time ks	Limit rate ct ks^{-1}	Lim. log f_X erg s^{-1} cm^{-2}	Lim. log L_X erg s^{-1}	log L_{bol} erg s^{-1}	log L_X/L_{bol}
10527	19.077	1.623	2.594	97.44	0.348	–14.48	28.77	31.7	–2.93
10547	14.64	1.012	1.063	196.72	0.24	–14.64	28.61	33.29	–4.68
10588	20.11	...	3.179	124.33	0.328	–14.51	28.75	31.48	–2.73
10606	19.275	1.565	2.556	42	0.754	–14.14	29.11	31.72	–2.61
10667	17.807	1.695	2.196	119.7	0.347	–14.48	28.77	31.97	–3.2
10723	13.664	0.783	0.965	213.75	0.244	–14.63	28.62	33.5	–4.88
10735	14.166	1.09	1.196	150.9	0.279	–14.58	28.68	33.1	–4.42
10736	12.043	0.668	0.763	62.92	0.643	–14.21	29.04	33.99	–4.95
10760	20.237	...	2.92	132.66	0.321	–14.52	28.74	31.57	–2.83
10768	18.022	...	2.331	166.14	0.272	–14.59	28.67	31.88	–3.21
10783	13.479	0.733	0.8	38.12	0.797	–14.12	29.13	33.93	–4.8
10796	20.088	...	2.917	34.24	0.716	–14.17	29.09	31.57	–2.48
10811	10.884	0.271	0.323	49.13	0.628	–14.22	29.03	34.64	–5.61
10832	21.532	...	3.552	61.96	0.665	–14.2	29.05	31.34	–2.29
10848	19.947	...	2.811	191.5	0.261	–14.6	28.65	31.6	–2.95
10877	21.256	...	3.36	194.03	1.988	–13.72	29.53	31.42	–1.89
11014	13.17	0.687	0.775	153.79	0.294	–14.55	28.7	33.97	–5.27
11029	14.801	1.051	1.124	195.66	0.267	–14.6	28.66	33.17	–4.51
11031	13.892	0.822	0.999	52.01	0.656	–14.21	29.05	33.39	–4.34
11039	20.733	...	3.021	162.83	0.881	–14.08	29.18	31.54	–2.36
11060	19.302	...	2.629	138.66	0.311	–14.53	28.72	31.68	–2.96
11136	20.278	...	3.026	40.42	0.651	–14.21	29.04	31.54	–2.5
11142	17.442	1.611	2.261	133.27	0.815	–14.11	29.14	31.93	–2.79
11195	19.685	...	2.711	109.92	0.426	–14.39	28.86	31.64	–2.78
11231	20.039	...	3.053	157.28	0.281	–14.57	28.68	31.53	–2.85
11235	18.101	1.445	-9.999	54.09	0.539	–14.29	28.96	32.57	–3.61
11287	18.38	...	2.357	121.38	2.211	–13.68	29.58	31.86	–2.28
11303	19.243	...	2.562	48.2	0.751	–14.15	29.11	31.71	–2.6
11304	14.282	0.928	1.007	176.17	0.299	–14.55	28.71	33.38	–4.67
11307	13.701	0.741	0.838	161.62	0.374	–14.45	28.8	33.85	–5.05
11363	17.845	1.583	2.249	15.78	0.904	–14.07	29.19	31.94	–2.75
11405	18.158	1.716	2.35	15.29	0.906	–14.06	29.19	31.87	–2.68
11441	14.552	0.942	1.078	91.86	0.355	–14.47	28.78	33.26	–4.48
11520	20.515	...	3.135	36.6	0.626	–14.23	29.03	31.5	–2.47
11549	15.091	1.075	1.19	160.13	0.291	–14.56	28.69	33.11	–4.42
11611	9.619	0.223	0.257	121.16	0.325	–14.51	28.74	34.74	–6
11634	17.665	1.666	2.047	44.22	0.761	–14.14	29.11	32.15	–3.04
11716	13.756	0.801	0.896	94.12	0.463	–14.36	28.9	33.71	–4.81
11729	14.762	1.024	1.143	36.2	0.643	–14.21	29.04	33.15	–4.11
11788	14.593	0.991	1.047	135.59	0.344	–14.49	28.77	33.31	–4.54
11813	20.824	...	3.422	118.05	0.799	–14.12	29.13	31.4	–2.27
11844	19.155	...	2.557	110.25	0.336	–14.5	28.76	31.72	–2.96
11852	19.377	...	2.594	99.5	0.344	–14.49	28.77	31.7	–2.93
11857	16.964	1.513	1.888	22.53	0.907	–14.06	29.19	32.38	–3.19
11906	19.423	...	2.651	35.24	0.694	–14.18	29.07	31.67	–2.6
11956	15.174	1.215	1.365	67.93	0.46	–14.36	28.89	32.91	–4.02
11969	17.868	1.545	2.153	19.05	1.139	–13.97	29.29	32.02	–2.73
11998	19.64	...	2.74	26.5	1.031	–14.01	29.24	31.62	–2.38
12109	15.308	1.101	1.206	16.4	1.318	–13.9	29.35	33.09	–3.74
12134	14.425	1.124	1.229	77.94	0.525	–14.3	28.95	33.06	–4.11
12206	19.447	...	2.613	93.27	0.443	–14.38	28.88	31.69	–2.81
12210	19.811	...	2.692	46.49	0.747	–14.15	29.1	31.65	–2.55
12216	12.879	0.683	0.813	16.35	1.299	–13.91	29.34	33.9	–4.56
12235	11.732	0.461	0.64	16.85	1.237	–13.93	29.32	34.19	–4.87
12244	20.471	...	2.873	32.44	0.665	–14.2	29.05	31.58	–2.53
12276	16.269	1.39	1.565	89.07	0.449	–14.37	28.88	32.72	–3.84
12362	14.385	1.092	1.176	65.74	0.495	–14.33	28.93	33.12	–4.19
12365	19.293	1.726	2.624	17.02	1.155	–13.96	29.29	31.68	–2.39
12416	10.135	0.205	0.261	36.11	0.736	–14.16	29.1	34.78	–5.68

Table C.1. continued.

Opt. Id.	V mag	$B-V$ mag	$V-I$ mag	Time ks	Limit rate ct ks^{-1}	Lim. log f_X erg s^{-1} cm^{-2}	Lim. log L_X erg s^{-1}	log L_{bol} erg s^{-1}	log L_X/L_{bol}
12451	16.862	1.452	1.808	70.67	0.638	–14.22	29.04	32.49	–3.45
12553	16.967	1.533	1.86	79.25	0.488	–14.33	28.92	32.42	–3.5
12565	15.489	1.217	1.295	63.34	0.53	–14.3	28.96	32.97	–4.01
12597	15.848	1.267	1.462	34.49	0.721	–14.16	29.09	32.83	–3.74
12600	16.561	1.491	2.015	49.97	0.784	–14.13	29.13	32.18	–3.05
12613	19.888	...	2.849	34.29	0.903	–14.07	29.19	31.59	–2.4
12628	14.507	...	1.135	64.28	2.727	–13.59	29.67	33.16	–3.49
12709	19.534	...	2.701	62.89	0.541	–14.29	28.96	31.64	–2.68
12711	19.631	...	2.777	46.54	0.782	–14.13	29.12	31.61	–2.49
12754	13.564	0.871	0.939	37.97	0.803	–14.12	29.14	33.58	–4.44
12802	16.177	1.27	1.547	43.16	0.797	–14.12	29.13	32.74	–3.61
12805	19.955	...	2.984	42.99	0.761	–14.14	29.11	31.55	–2.44
12835	17.275	1.433	1.971	36.8	0.961	–14.04	29.21	32.22	–3.01
12868	16.668	1.492	2.134	36.35	0.841	–14.1	29.16	32.05	–2.89
12909	11.027	0.345	0.439	35.76	0.834	–14.1	29.15	34.47	–5.32
13065	17.474	1.519	2.079	21.35	0.969	–14.04	29.22	32.11	–2.89
13079	17.825	1.468	2.249	21.15	1.008	–14.02	29.23	31.94	–2.71
13342	19.378	...	2.64	13.4	0.938	–14.05	29.2	31.68	–2.48
13349	14.903	1.035	1.182	13.4	0.974	–14.03	29.22	33.11	–3.89
8947	17.87	1.521	2.306	244.55	2.089	–13.7	29.55	31.9	–2.35
5877	13.852	0.891	0.995	107.32	1.034	–14.01	29.25	33.4	–4.15
5563	11.928	0.516	0.641	16.79	0.861	–14.09	29.17	34.19	–5.02
9869	18.449	1.591	2.371	53.11	0.634	–14.22	29.03	31.85	–2.82
8328	17.898	1.531	2.22	85.5	0.437	–14.38	28.87	31.96	–3.09
11243	15.724	1.264	1.376	177.94	0.299	–14.55	28.71	32.9	–4.19
7870	20.956	...	3.201	280.02	0.19	–14.74	28.51	31.48	–2.97
11823	20.089	...	2.891	119.81	0.406	–14.41	28.84	31.58	–2.74
5130	14.299	0.925	1.001	78.3	0.453	–14.37	28.89	33.39	–4.5
6683	19.031	...	2.479	103.97	0.329	–14.51	28.75	31.75	–3
5586	12.689	0.624	0.742	15.17	1.306	–13.91	29.35	34.03	–4.68
6745	18.471	1.676	2.602	45.67	0.867	–14.08	29.17	31.69	–2.52
15497	8.78	0.09	...	126.83	4.285	–13.5	29.75	35.19	–5.44
15498	8.06	-0.02	...	31.37	0.736	–14.27	28.98	36.9	–7.92
15502	9.05	0.08	...	230.59	1.848	–13.87	29.38	35.27	–5.89
15514	8.93	0.04	...	11.95	1.436	–13.98	29.27	36	–6.73
15515	8.52	0.05	...	126.35	0.342	–14.6	28.65	35.53	–6.88
15517	7.73	0.03	...	203.47	0.222	–14.79	28.46	36.21	–7.75
15518	9.18	0.12	...	114.32	0.297	–14.66	28.59	35.03	–6.44
15519	9.43	0.06	...	84.6	0.364	–14.58	28.68	35.45	–6.77
15520	6.87	-0.01	...	183.27	0.287	–14.68	28.57	36.75	–8.18
15521	9.03	0.05	...	260.87	0.192	–14.85	28.4	35.53	–7.13
15522	8.55	0.07	...	198.06	0.721	–14.28	28.97	35.34	–6.37
15523	9.6	0.11	...	266.02	0.409	–14.53	28.73	35.09	–6.36
15524	9.67	0.08	...	199.24	0.572	–14.38	28.87	35.27	–6.4
15525	7.64	–0.06	...	124.95	0.28	–14.69	28.56	...	...
15526	6.71	1.28	...	261.52	0.171	–14.9	28.35	32.81	–4.46
15527	7.23	0.05	...	264.91	0.168	–14.91	28.34	35.53	–7.19
15528	8.21	0.02	...	238.6	0.264	–14.71	28.54	36.35	–7.81
15529	8.57	0.05	...	291.55	0.152	–14.95	28.3	35.53	–7.23
15530	8.76	0.04	...	235.53	0.181	–14.88	28.37	36	–7.63
15531	9.65	0.11	...	97.6	0.368	–14.57	28.68	35.09	–6.41
15533	7.85	0.03	...	240.98	0.245	–14.75	28.51	36.21	–7.7
15534	9.56	0.16	...	180.84	0.286	–14.68	28.57	34.9	–6.33
15535	8.38	0.04	...	69.38	0.471	–14.46	28.79	36	–7.21
15536	5.19	1.76	...	47.5	0.56	–14.39	28.86	31.54	–2.68
15538	8.39	0	...	118.31	0.334	–14.61	28.64	36.54	–7.9
15539	9.21	0.11	...	86.29	3.223	–13.63	29.62	35.09	–5.47
15541	9.4	0.11	...	277.15	0.194	–14.85	28.4	35.09	–6.69
15543	9.45	0.08	...	153.48	0.278	–14.69	28.56	35.27	–6.71

Table C.1. continued.

Opt. Id.	V mag	$B-V$ mag	$V-I$ mag	Time ks	Limit rate ct ks^{-1}	Lim. log f_X erg s^{-1} cm^{-2}	Lim. log L_X erg s^{-1}	log L_{bol} erg s^{-1}	log L_X/L_{bol}
15544	9.48	0.07	...	260.53	0.204	–14.83	28.43	35.34	–6.91
15545	9.56	0.18	...	77.18	0.478	–14.46	28.8	34.85	–6.05

Appendix D: Finding charts of unidentified sources

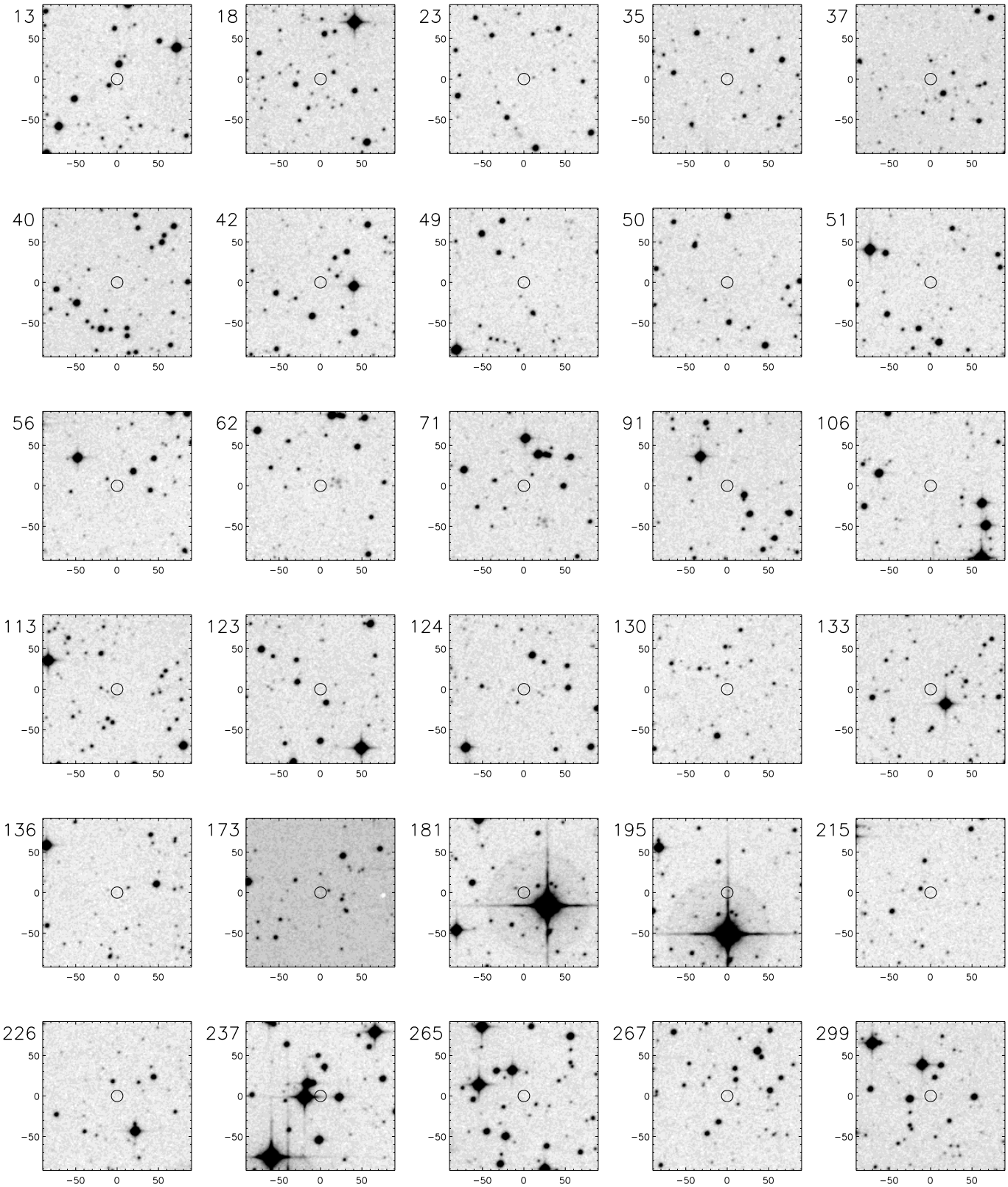

Fig. D.1. DSS IR finding charts (3′ × 3′ side) at the position of unidentified X-ray sources.

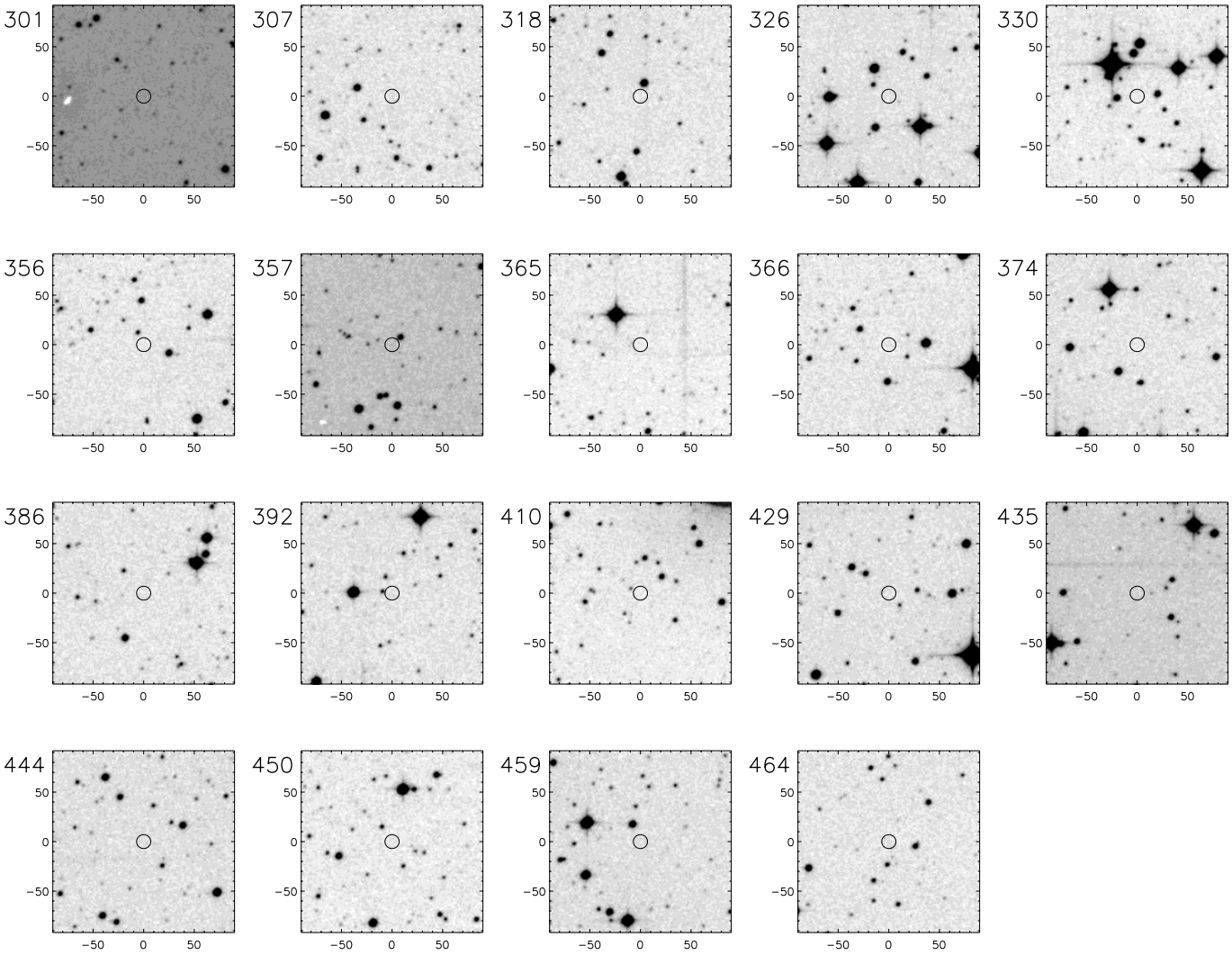

Fig. D.2. As in Fig. D.1.